



Research article

Magnetic poly(1,8-diaminonaphthalene)-nickel nanocatalyst for the synthesis of antioxidant and antibacterial isoxazole-5 (4H)-ones derivatives

Shefa Mirani Nezhad, Seied Ali Pourmousavi, Ehsan Nazarzadeh Zare^{*},
Golnaz Heidari, Samanesadat Hosseini, Mahla Peyvandtalab

School of Chemistry, Damghan University, Damghan, 36716-45667, Iran

ARTICLE INFO

Keywords:

Poly(1,8-diaminonaphthalene)-nickel
Nanocatalyst
Isoxazol-5(4H)-Ones
Bioactive

ABSTRACT

A magnetic poly (1,8-diaminonaphthalene)-nickel (PDAN-Ni@Fe₃O₄) composite as a multifunctional nanocatalyst was prepared in several steps including (I) synthesis of poly (1,8-diaminonaphthalene) (PDAN), (II) modification of PDAN with NiSO₄ (PDAN-Ni) and (III) preparation of magnetic nanocatalyst by iron (I and II) salts in the existence of PDAN-Ni complex (PDAN-Ni@Fe₃O₄). Fourier-transform infrared spectroscopy (FTIR), elemental analysis (CHNSO), vibrating-sample magnetometer (VSM), X-ray diffraction (XRD), energy-dispersive X-ray (EDX), field emission scanning electron microscope (FESEM), ultraviolet-visible (UV-vis), and thermogravimetric analysis (TGA) were applied to characterize the prepared nanocatalyst. The PDAN-Ni@Fe₃O₄ was applied as an environmentally friendly nanocatalyst for the isoxazole-5(4H)-ones synthesis via a one-pot reaction between aryl/heteroaryl aldehyde, hydroxylamine hydrochloride, and β-ketoester. The nanocomposite was also used for the synthesis of some new alkylene bridging bis 4-benzylidene-3-methyl isoxazole-5(4H)-ones. The catalyst's reusability, and the antioxidant and antibacterial activities of both catalyst and products, were studied. Results showed that the nanocatalyst and isoxazole-5(4H)-ones have antioxidant activity of 75% and 92%, respectively. In addition, the antibacterial test showed that the nanocatalyst and isoxazole-5(4H)-ones have highly active versus *Staphylococcus aureus* and *Escherichia coli* bacteria. The reusability and stability of the nanocatalyst, a medium to higher product yield and conversion, a faster reaction time, and the use of green solvents were a few benefits of this study.

1. Introduction

Heterocyclic compounds and their production are important to medicinal chemists because they help them to develop more active pharmaceutical compounds [1–3]. On the other hand, developing a non-hazardous synthetic technique to create heterocyclic substances that are bioactive is a critical task in the current situation [4,5]. Nowadays, multi-component reactions are a simple and clean way to make bioactive heterocyclic chemicals in organic chemistry. These reactions are attractive to chemists because they have features such as high conversion efficiency, environmental friendliness, ease, and fast, and do not require column chromatography [6, 7].

^{*} Corresponding author.E-mail addresses: ehsan.nazarzadehzare@gmail.com, e.nazarzadeh@du.ac.ir (E.N. Zare).<https://doi.org/10.1016/j.heliyon.2023.e15886>

Received 20 December 2022; Received in revised form 21 April 2023; Accepted 25 April 2023

Available online 4 May 2023

2405-8440/© 2023 Published by Elsevier Ltd.

This is an open access article under the CC BY-NC-ND license

<http://creativecommons.org/licenses/by-nc-nd/4.0/>.

Nitrogen- and oxygen-containing heterocyclic compounds like isoxazoles and their derivatives are widely used in medicine and have many biological and industrial applications, including analgesic and anti-androgens, *anti*-HIV, analgesic, anti-tubercular, anti-viral, antiprotozoal, antioxidant, antitumor, antifungal, antibacterial, anti-inflammatory, immunosuppressive, adrenergic receptor antagonists, etc. Fig. 1 depicts several biologically active isoxazole derivatives [8–14].

There are several ways to make substituted isoxazole-5(4*H*)-ones, such as the reaction of β -ketoesters with hydroxylamine in the presence of NaOH [15], benzaldoximes and 1,3-dicarbonyl condensation [16], Knoevenagel reaction between ethyl acetoacetate and hydroxylamine hydrochloride [17], cyclization of *o*-propionyl oximes [18]. Isoxazoles could be made through homogeneous and heterogeneous catalysts. For example, Cu₂O nanocrystals as heterogeneous catalysts for the production of isoxazoles were investigated for their facet-dependent catalytic potential [19]. The metal-catalyzed alkynes are described as a route to the synthesis of isoxazoles [20]. Furthermore, other studies reported the use of intensified sun radiation in the production of 3-methyl-4-aryl methylene isoxazole-5(4*H*)-ones [21].

Metal and organometallic compounds are well recognized for their widespread application in both academic and industry research [22]. The complexes of transition metal and organometallic with great selectivity and efficiency in any reaction environment are commonly used as homogeneous catalysts. In practice, catalysts separating from the reaction is hard because of waste formation [23]. However, it is generally agreed that heterogeneous catalysts provide significant technical benefits over their homogeneous counterparts. Additionally, conventional solid acid catalysts such as silica-based solid acids [1], ion exchange resins [2], molecular sieves [3], metal oxide nanoparticles [24], and carbon-based solid acids [4] require time-consuming preparation, have limited activity, and have poor stability. Thus, there will be a need for a catalyst with high stability, activity, and ease of isolation.

Stabilization or covalent binding of the catalyst on the surface of the support increases its availability to carry out chemical reactions more effectively. The separation and recycling of costly catalyst nanoparticles are only two examples of the many possible uses for magnetic nanoparticles, which have garnered increasing attention among the many nanostructured materials available [25]. The employing of magnetic nanomaterials in heterogeneous catalysis has been reported by others. For example, modified chitosan through Cu(II)-5-amino-1*H*-tetrazole was employed for the C–N coupling reaction [26], for the Sonogashira coupling process, Pd nanoparticles supported on the modified chitosan-kaolin were utilized as a catalyst [27], magnetic lanthanide-based MOF supported on sea sponge was used for the hydrogenation reaction [28], magnetic palladium nanoparticles were applied in Suzuki cross-coupling reaction [25], graphene oxide/Cu-MOF-magnetic nanocomposite was employed in the ciprofloxacin degradation [29].

Nanocatalysts with high functionality are beneficial materials for multi-component reactions. The use of nanostructures with active sites has developed as a key option in catalyst design [30]. One route to fabricate multifunctional catalysts is to use polymers as a

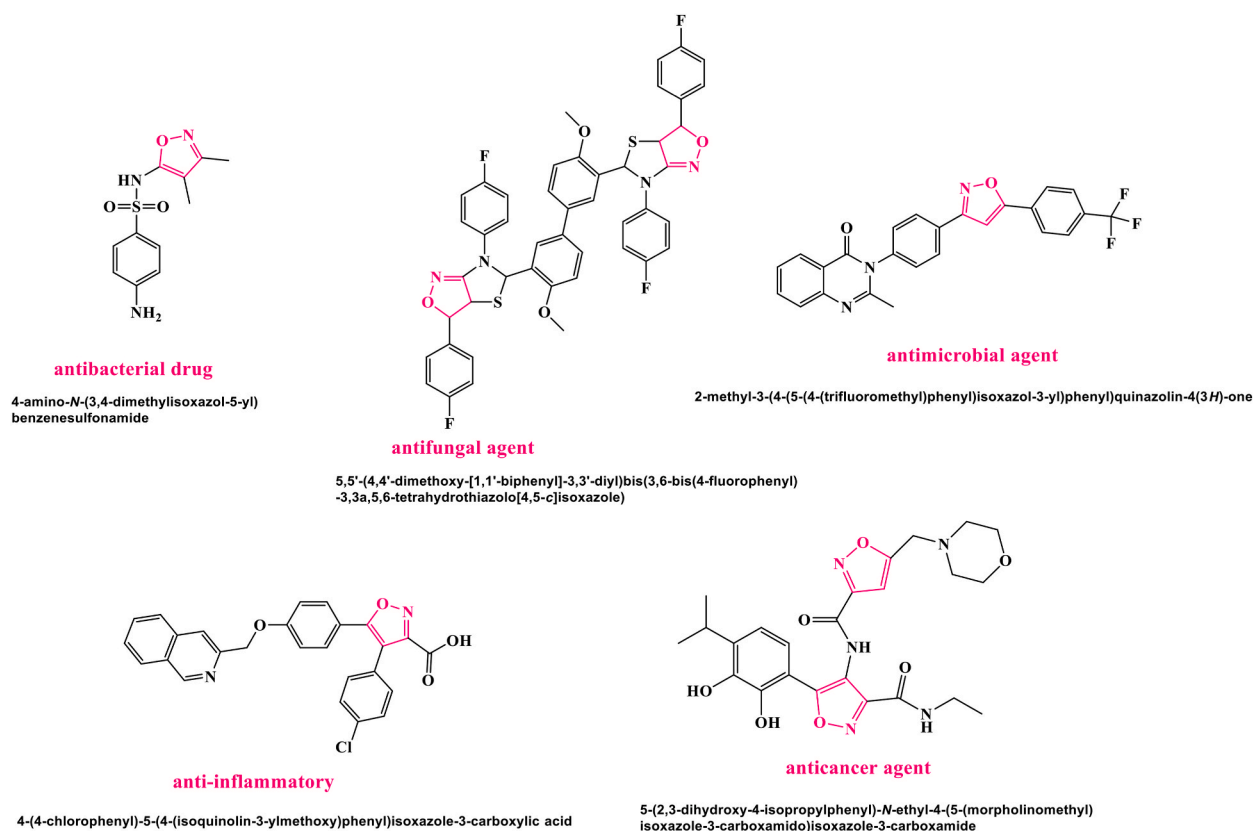


Fig. 1. Isoxazole compounds with the biological activity.

high-functionality matrix. Lately, polymer-based catalysts due to their high functionality, easy separation, and good compatibility employed in various organic reactions. Aromatic amine polymers, such as poly (diaminonaphthalene) (PDAN) and poly (1,8-diaminonaphthalene), are predominantly organic compounds with extended single and double bonds alternating in a p-orbital system. The imine, and amine groups in the PDAN structure make this polymer an ideal option in catalytic chemistry [31]. Generally, to create diaminonaphthalene (DAN), the -NH_2 group is substituted at various sites in the second benzene ring of naphthalene [32]. Metal ions can create stable complex derivatives with these main free amine groups [33]. As a result, the complexation of PDAN with nickel is a way to make component activation easier in the isoxazole synthesis process. On the other side, a magnetic catalyst can not only preserve its catalytic activity after several recycles, but it can also cut manufacturing costs by facilitating the catalytic reaction's post-treatment procedure by magnetic separation [34–36].

There is no literature concerning the employ of magnetic poly (1,8-diaminonaphthalene)-nickel nanocatalyst in the synthesis of bioactive isoxazole-5(4H)-ones. Therefore, the goal of the current study is the preparation of the multifunctional magnetic poly (1,8-diaminonaphthalene)-nickel nanocatalyst and its employ in the synthesis of bioactive isoxazole-5(4H)-ones under mild and green conditions. The reusability of the catalyst, as well as the antioxidant and antibacterial activity of both catalyst and products, are further investigated. A medium to higher product yield and conversion, a faster reaction time, and less use of strong solvents are some advantages of the current study.

2. Experimental

2.1. Materials

1,8-diaminonaphthalene, ferrous chloride, ferric chloride, ammonium persulfate, nickel sulfate hexahydrate, ammonia solution 25%, all solvents, β -ketoesters, hydroxylamine hydrochloride, and everything else was supplied the German chemical company, Merck.

2.2. Preparation of magnetic poly (1,8-diaminonaphthalene)-Ni catalyst

Magnetic poly (1,8-diaminonaphthalene)-Ni (PDAN-Ni@Fe₃O₄) catalyst was fabricated in three steps as follows:

First step: at room temperature, 0.791 g (5 mmol) of 1,8-diaminonaphthalene was dissolved in acetonitrile (50 mL) inside a glass flask that had a volume of 200 mL. To make an oxidant solution, 1.14 g (5 mmol) of (NH₄)₂S₂O₈ was dissolved in a volume of 50 mL of distilled water. Following the stirring step, the monomer solution was mixed with 50 mL of the oxidant solution. To eliminate the remaining oxidant and water-soluble oligomers, the precipitate was filtered and extensively washed with distilled H₂O. Finally, the solid polymer was dried for 24 h in an oven at 50 °C (Fig. 2A).

Second step: 1 g of poly (1,8-diaminonaphthalene) and 0.5 g of NiSO₄·(H₂O)₆ were added to a 10 mL methanol to form nickel complexes with amine groups of the polymer, and the mixture was mechanically agitated under reflux over 12 h. To eliminate the leftover NiSO₄·(H₂O)₆, the obtained precipitate was washed with deionized H₂O and MtOH. The PDAN-Ni was vacuum dried at 50 °C for 12 h (Fig. 2B).

Third step: the in-situ co-precipitation approach was used to make a magnetic PDAN-Ni@Fe₃O₄ nanocomposite from a solution of Fe(II) and Fe(III) salts, and PDAN-Ni (Fig. 2C). FeCl₂·4H₂O (0.0049 mol) and FeCl₃·6H₂O (0.00210 mol) salts were dissolved in 25 mL of deionized H₂O while the temperature was kept at 25 °C. The mixture was then mechanically agitated at 80 °C for 30 min after adding 1 g of PDAN-Ni to the solution. The mixture was immediately added to NH₄OH (25%) (10 mL) till the pH reached 10–12. After 30 min, the precipitate was collected by magnetic and washed with H₂O and EtOH. Eventually, in an oven set at 80 °C for 12 h, the PDAN-Ni@Fe₃O₄ nanocomposite was dried.

2.3. Synthesis of isoxazole-5(4H)-ones

1 mmol of aryl/heteroaryl aldehyde, 1 mmol of β -ketoester, 1 mmol of hydroxylamine hydrochloride, and 0.04 g of PDAN-Ni@Fe₃O₄ were added to 5 mL of distilled H₂O in the reaction container and agitated at 50 °C. After the reaction was finished, the PDAN-Ni@Fe₃O₄ was extracted employing a magnet, and the product was removed by simple filtering. EtOH (95%) was used in a crystallization process to separate impurities from the product (Fig. 2D).

2.4. Synthesis of bis(4-benzylidene-3-methyl)isoxazole-5(4H)-ones using alkylene bridges

β -Ketoester (2 mmol), hydroxylamine hydrochloride (2 mmol), and the PDAN-Ni@Fe₃O₄ (0.04 g) were mixed in the 5 mL of H₂O/EtOH (50:50). Subsequently, the solution was added to the flask and stirred at 50 °C until the reaction was finished. Afterward, alkylene bridging hydroxybenzaldehyde (1 mmol) was added to the mixture and stirred till the reaction was finished. The catalyst was isolated by a magnet after the reaction was finished, and the precipitate was removed by simple filtering. To obtain pure compounds, the products were crystallized using EtOH.

2.5. Synthesis of 3-methyl-1-phenyl-1H-pyrazole-5-ol

The reaction flask was filled with a combination of acetic acid (0.5 mL), phenylhydrazine (0.05 mol, 5 mL), and ethyl acetoacetate

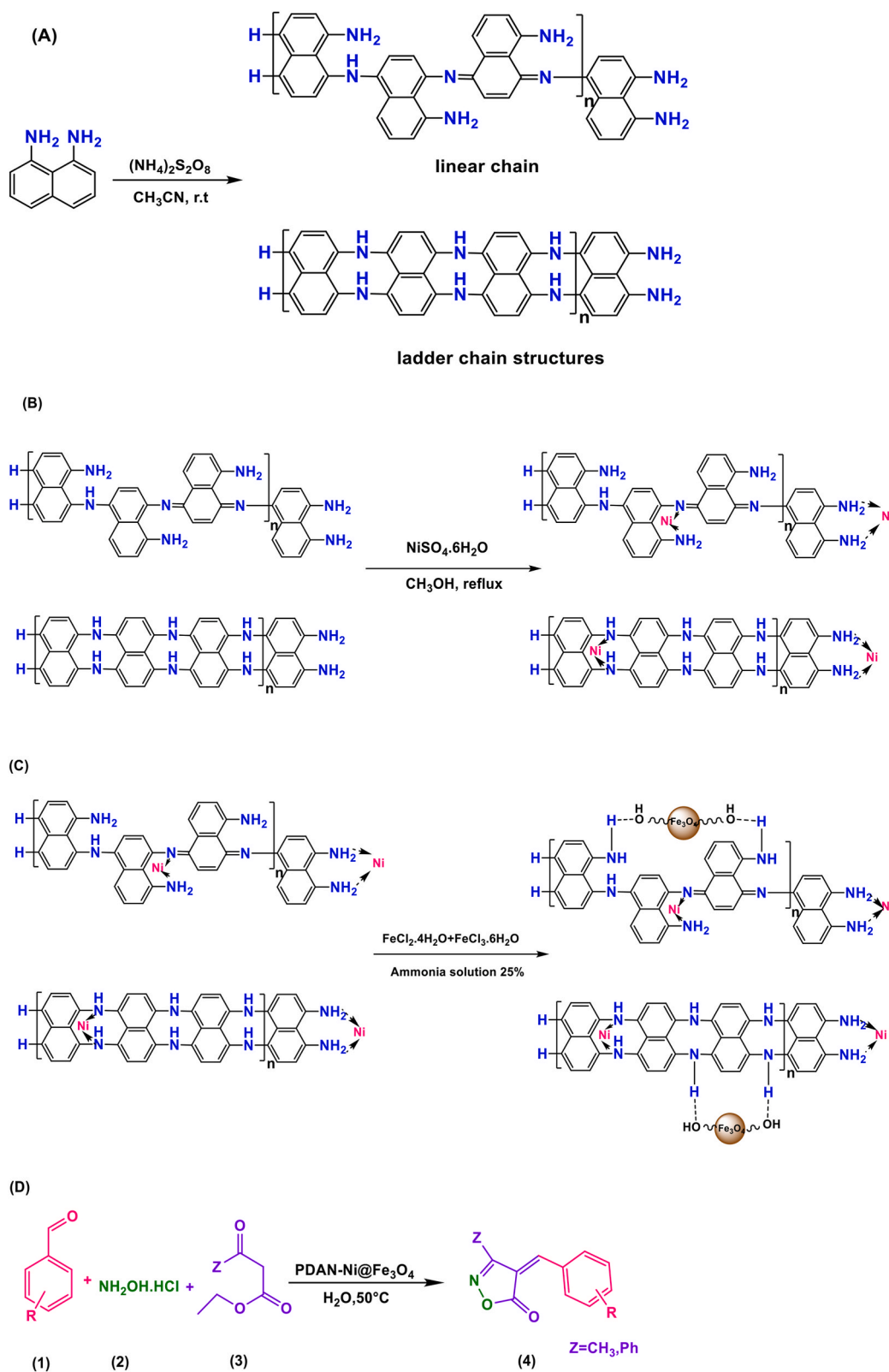


Fig. 2. Preparation of poly(1,8-diaminonaphthalene) (A), poly(1,8-diaminonaphthalene)-Ni (B), poly(1,8-diaminonaphthalene)-Ni@Fe₃O₄ (C), and synthesis of isoxazole-5(4H)-ones (D).

(0.05 mol, 6.2 mL), and heated to 90 °C for 60 min while being stirred. EtOH was used for crystallization once the liquid had cooled to 25 °C and 10–20 mL ether had been added to the mixture and filtered to remove the precipitate [37].

2.6. Synthesis of bis-pyrazolone

5 mL of EtOH, 1 mmol of 3-methyl-1-phenyl-3-methyl-5-pyrazolone, and 0.04 g of PDAN-Ni@Fe₃O₄ were introduced to a flask containing an isoxazole 5(4H) one derivative while it was being stirred at 80 °C. The PDAN-Ni@Fe₃O₄ was afterward removed using a magnet, and the result was filtered and EtOH–H₂O before being collected.

2.7. Characterization

The following instruments were applied for samples characterization.

CHNSO elemental analyzer (Elementar Vario El (III), Germany), hydrogen and carbon nuclear magnetic resonance spectroscopy (1HNMR and 13CNMR, Bruker Avance DRX-400, Bremen, Germany), Fourier transform infrared spectroscopy (FTIR, Bruker Tensor 27, Bremen, Germany), energy dispersive X-Ray (EDX) (MFTIRA III, TESCAN, Czech Republic), field emission scanning electron microscope, X-ray diffraction (XRD, Shibuya-ku, Tokyo, Japan), thermogravimetric analysis (TGA 209F3, NETZSCH, Selb, Germany), ultraviolet–visible spectroscopy (UV–vis, Cecil 5000 series, Cambridge, UK) and vibrating-sample magnetometer (VSM, LKBFB, Meghnatis Daghigh. Kavir Co, Kashan, Iran).

3. Results and discussions

3.1. Polymer-based catalyst characterization

Elemental analysis: The description of the PDAN, PDAN-Ni, and PDAN-Ni@Fe₃O₄ nanocomposite was investigated via CHNSO (Table 1). (NH₄)₂S₂O₈ incorporated in the polymer matrix led to a negligible amount of sulfur and oxygen components in the PDAN. The increase of oxygen and sulfur elements in the PDAN-Ni is related to NiSO₄·(H₂O)₆. The existence of Fe₃O₄ in the nanocomposite is observed with increasing oxygen content in the structure of PDAN-Ni @Fe₃O₄ compared to PDAN-Ni.

FTIR: Fig. 3A displays the FTIR spectra of the PDAN, PDAN-Ni, and PDAN-Ni@Fe₃O₄ nanocomposite. The PDAN's FTIR spectrum reveals the NH₂ and N–H stretching vibrations at 3454 cm⁻¹. The C–H stretching vibration is associated with the existence of a minor peak at 2940 cm⁻¹. Stretching vibrations of C=N and C=C bonds on quinoid rings are reflected in a large absorption band at 1650 cm⁻¹. The emergence of the band at 1260 cm⁻¹ confirms the presence of C–N and C–H bonds. C–H bending modes detected at 815 cm⁻¹, which are out-of-plane stretches [38]. In the FTIR spectrum of PDAN-Ni, the C=N and –NH₂ stretching vibrations of the PDAN shifted from 1650 cm⁻¹ to 1612 cm⁻¹ (red-shifted) and 3454 cm⁻¹ to 3426 cm⁻¹, respectively which indicates a coordination link between the imino and amine nitrogen atoms of PDAN and the nickel. The addition of Fe₃O₄ nanoparticles has resulted in a noticeable change in several FTIR bands in the spectrum of the PDAN-Ni@Fe₃O₄. At 634 cm⁻¹, Fe₃O₄ exhibits the Fe–O–Fe stretching modes.

UV–vis: Fig. 3B shows the UV–vis spectra of PDAN and PDAN-Ni. A significant absorbance peak at 300 nm is associated with the π–π* transitions of the benzenoid ring in the UV–vis spectra of PDAN. The benzenoid-to-quinoid interbond charge transfer or π–π*

Table 1

Elemental analysis data of the PDAN, PDAN-Ni, and PDAN-Ni@Fe₃O₄ nanocomposite. The values in parentheses represent the calculated.

SAMPLES	C%	H%	N%	S%	O%
PDAN	67.96 (75.92)	5.89 (6.37)	21.11 (17/71)	1.20 (–)	4.05 (–)
PDAN-Ni	59.35	4.45	16.30	2.72	12.04
PDANNi@Fe ₃ O ₄	39.35	3.40	13.29	1.90	29.05

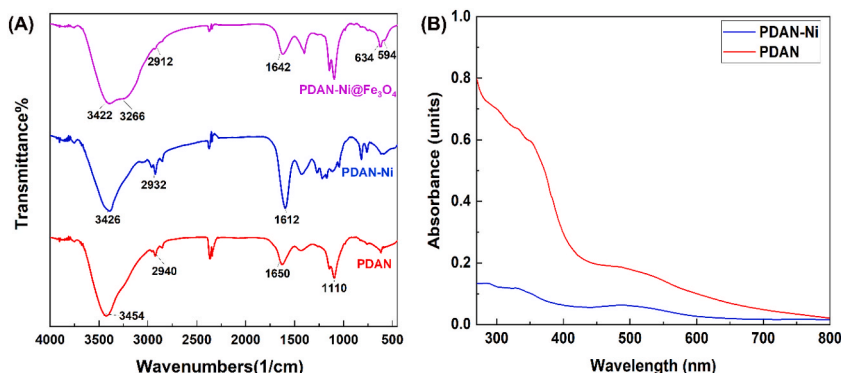


Fig. 3. FTIR spectra (A), UV–vis spectra of PDAN and PDAN-Ni in DMSO solvent (B).

excitation band is responsible for the wide absorbance peak between 477 and 529 nm [39]. In the UV–vis spectrum of PDAN-Ni, the absorption intensity has decreased compared to the PDAN. This decrease in absorption is related to the formation of a complex between nickel ions and amine groups in the PDAN. This result has already been described by researchers who expressed that the absorption strength decreases with proceeding complex formation [40,41].

VSM: VSM is a technique for figuring out a material's magnetic characteristics. Fig. 4A shows that the VSM curve of the PDAN-Ni@Fe₃O₄ had an S-like with coercivity (Hc) and remanence (Mr) equally zero, which confirms its superparamagnetic property. Furthermore, the magnetic property of PDAN-Ni@Fe₃O₄ was obtained by the saturation value of 30.57 emu/g.

TGA: To examine the thermal stability of samples, the TGA was used. The thermograms of the PDAN, PDAN-Ni, and PDAN-Ni@Fe₃O₄ nanocomposite are exposed in Fig. 4B. The mass loss below 200 °C associated with the elimination of humidity sorbed on the samples. The oligomer elimination and the failure of the polymer's main chains caused the second and third mass losses, respectively. The thermograms of PDAN, PDAN-Ni, and PDAN-Ni@Fe₃O₄ nanocomposite revealed that PDAN-Ni and PDAN-Ni@Fe₃O₄ were more stable than PDAN, which is due to the coordination interaction between PDAN and nickel, as well as the robust interaction between the –OH of Fe₃O₄ nanoparticles and the –NH₂ on the PDAN-Ni@Fe₃O₄.

X-ray diffraction: Fig. 5 displays the XRD patterns of the PDAN, PDAN-Ni, and PDAN-Ni@Fe₃O₄ nanocomposite. The XRD pattern of PDAN revealed a large peak, which is indicative of the substance's amorphous nature. The complexation of Ni with the –NH₂ groups of the PDAN caused the XRD pattern of PDAN-Ni to have a semicrystalline character. This outcome was quite consistent with other results that were published [39]. The XRD pattern of the PDAN-Ni@Fe₃O₄ nanocomposite had a crystalline character because Ni and Fe₃O₄ nanoparticles were present in the PDAN matrix.

EDX: As seen in Fig. 6A, the chemical structure of the PDAN, PDAN-Ni, and PDAN-Ni@Fe₃O₄ nanocomposite was also specified with EDX analysis. The evaluation of spectra and tabular data demonstrated the existence of varied quantities of the atoms O, C, N, and S. The existence of S in PDAN is due to (NH₄)₂S₂O₈ trapped in the polymer, whereas in PDAN-Ni and PDAN-Ni@Fe₃O₄ is related to the NiSO₄. Furthermore, the presence of Ni in the PDAN-Ni sample suggests that a coordination connection between the imino and amine

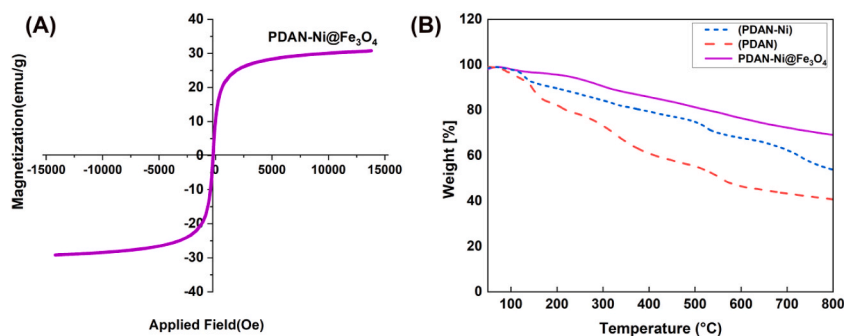


Fig. 4. VSM curve of the PDAN-Ni@Fe₃O₄ (A), TGA thermograms of the prepared PDAN, PDAN-Ni, and PDAN-Ni@Fe₃O₄ (B).

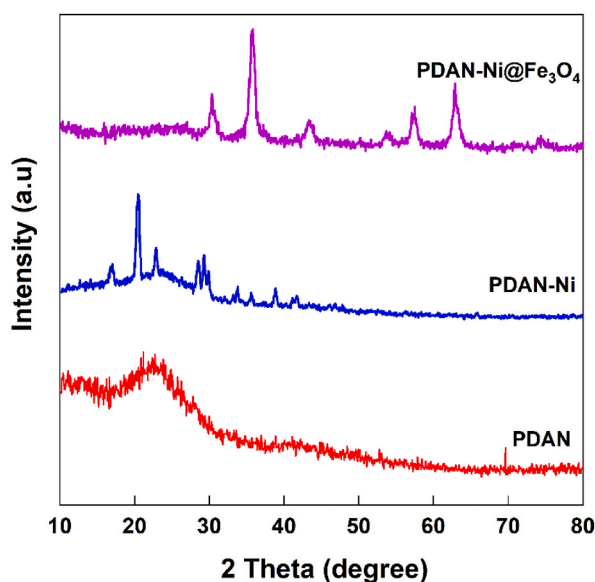


Fig. 5. XRD patterns of the PDAN, PDAN-Ni, and PDAN-Ni@Fe₃O₄.

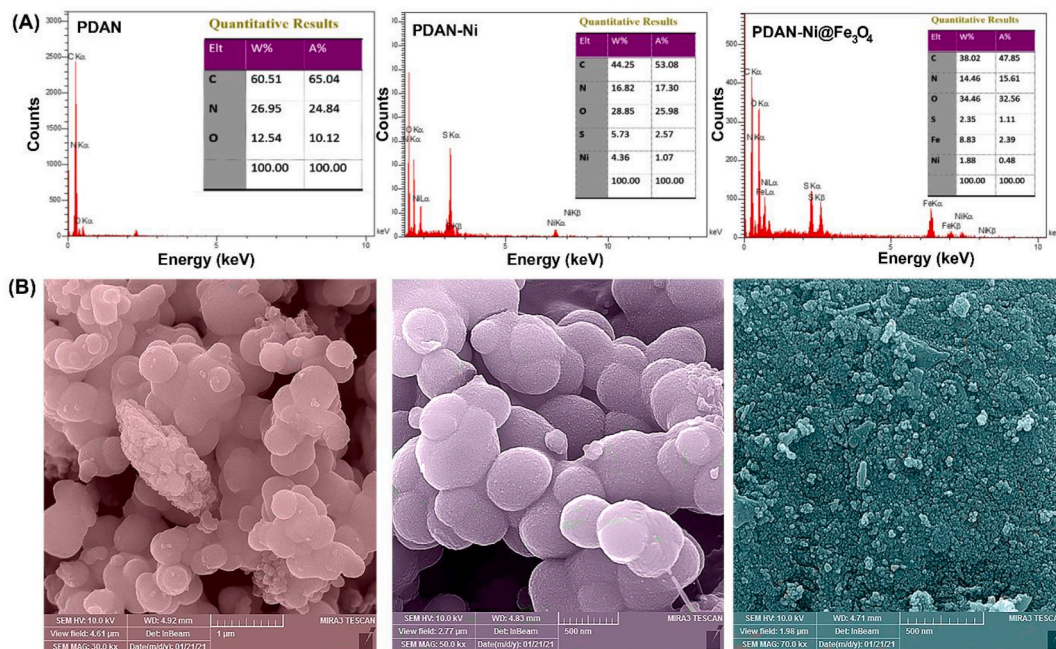


Fig. 6. EDX spectra (A), and FESEM micrographs (B) of the PDAN, PDAN-Ni, and PDAN-Ni@Fe₃O₄ nanocomposite.

nitrogen atoms of PDAN and the nickel occurred, and the presence of Fe in the PDAN-Ni@Fe₃O₄ specifies that the Fe₃O₄ in the composite exists.

FESEM: Fig. 6B displays the FESEM images of PDAN, PDAN-Ni, and PDAN-Ni@Fe₃O₄ in magnifications of 1 μm and 500 nm, respectively. An aggregation of spherulike particles was detected in the FESEM images of PDAN, PDAN-Ni, and PDAN-Ni@Fe₃O₄. In addition, the images showed that the particle size in the PDAN-Ni@Fe₃O₄ was smaller than the PDAN, PDAN-Ni. The average particle size diameter of PDAN-Ni@Fe₃O₄ was between 30 nm and 50 nm. These results exposed that the PDAN-Ni@Fe₃O₄ was magnificently prepared.

3.2. Investigation the catalytic activity of PDAN-Ni@Fe₃O₄

In order to check the catalytic activity of PDAN-Ni@Fe₃O₄, first, we investigate the isoxazole-5(4H)-ones synthesis via ethyl acetoacetate, hydroxylamine, aromatic aldehyde, and hydrochloride (Fig. 2D). The reaction optimization was attained through the reaction of, ethyl acetoacetate, vanillin, and hydroxylamine hydrochloride in different conditions (Table 2).

Table 2

Reaction optimization of vanillin, ethyl acetoacetate, and hydroxylamine hydrochloride under different conditions.^a

Entry	Solvent	Catalyst	Temp/°C	Time (Min)	Yield % ^b
1	EtOH	PDAN-Ni@Fe ₃ O ₄ (0.02)	R.T.	70	70
2	H ₂ O	PDAN-Ni@Fe ₃ O ₄ (0.02)	R.T.	70	89
3	THF	PDAN-Ni@Fe ₃ O ₄ (0.02)	R.T.	180	55
4	Hexane	PDAN-Ni@Fe ₃ O ₄ (0.02)	R.T.	180	20
5	CHCl ₃	PDAN-Ni@Fe ₃ O ₄ (0.02)	R.T.	180	45
6	solvent-free	PDAN-Ni@Fe ₃ O ₄ (0.02)	R.T.	180	75
7	H ₂ O/EtOH	PDAN-Ni@Fe ₃ O ₄ (0.02)	R.T.	70	85
8	H ₂ O	PDAN-Ni@Fe ₃ O ₄ (0.02)	50	60	92
9	H ₂ O	PDAN-Ni@Fe ₃ O ₄ (0.02)	Reflux	60	90
10	H ₂ O	PDAN-Ni@Fe ₃ O ₄ (0.04)	50	25	95
11	H ₂ O	PDAN-Ni@Fe ₃ O ₄ (0.06)	50	20	96
12	H ₂ O	–	50	180	60
13	H ₂ O	PDAN-Ni (0.04)	50	30	92
14	H ₂ O	PDAN (0.04)	50	35	90
15	H ₂ O	Fe ₃ O ₄ (0.04)	50	45	75
16	H ₂ O	NiSO ₄ (0.04)	50	45	80

^a Reaction conditions: Vanillin (1 mmol), ethyl acetoacetate (1 mmol), hydroxylamine hydrochloride (1 mmol), 5 mL water, and PDAN-Ni@Fe₃O₄ (0.04 g) at 50 °C.

^b Isolated yield. R.T., room temperature.

First, several solvents and solvent-free conditions were used to study the reaction (Table 2, entries 1–7). As seen in Table 2, H₂O was a more suitable solvent than other solvents. In addition, insignificant yields were given in less polar solvents like CH₃Cl, THF, and *n*-hexane (Table 2, entries 3–5). The efficiency of EtOH is relative to H₂O was also examined. Even though comparable products were observed (Table 2, entry 1), H₂O had a bordering gain, consequently showing to be the greatest medium for the reaction. The best conditions for the synthesis of intermediates (such as oxime and 3-methylisoxazole-5-ol) and their alteration to end products may be provided by H₂O that disperses heat more rapidly [42].

On the contrary, our findings indicated that the reaction requires a catalyst to proceed and that the yield is low without a catalyst (Table 2, entries 8–12). We examined the conversion rates in the existence of NiSO₄, Fe₃O₄, PDAN, PDAN-Ni, and PDAN-Ni@Fe₃O₄ (Table 2 entries 1–16). The best result was attained in PDAN-Ni@Fe₃O₄ as a catalyst with the lowest time and highest efficiency. The effect of temperature was also examined (Table 2 entries 1–16) so that 50 °C was the best temperature for the acting of reaction. The results showed that the best conditions are: vanillin (1 mmol), ethyl acetoacetate (1 mmol), hydroxylamine hydrochloride (1 mmol) in the existence of PDAN-Ni@Fe₃O₄ nanocatalyst (0.04 g) and H₂O as solvent at 50 °C.

Several aromatic aldehydes to produce a large range of isoxazole-5(4H)-ones were evaluated in the existence of 0.04 g PDAN-Ni@Fe₃O₄ (Table 3). As an overall tendency, the reaction was tolerant to a large variety of benzaldehyde derivatives including electron-withdrawing and -donating groups. The resulting compounds were purified by crystallization in ethanol and characterized using spectroscopic techniques (¹H NMR and FTIR). According to the findings in Tables 3 and it was possible to convert electron-donating group-containing benzaldehyde derivatives into their corresponding isoxazole 5(4H) derivatives with high to outstanding yields.

On the other hand, under ideal reaction circumstances, electron-withdrawing benzaldehyde derivatives were ineffective and did not proceed.

Alternatively, the synthesis of alkylene bridging bis 4-benzylidene-3-methyl isoxazole-5(4H)-one was accomplished utilizing bis aldehydes that bridge alkenes, ethyl acetoacetate, and hydroxylamine hydrochloride in the existence of PDAN-Ni@Fe₃O₄ at 50 °C. In technique, several novel alkylene bridging bis 4-benzylidene-3-methyl isoxazole-5(4H)-ones (5 a-d in Fig. 7) were synthesized for the first time.

Suggested mechanism: Fig. 8 shows the possible mechanism for the isoxazole 5(4H) ones synthesis by PDAN-Ni@Fe₃O₄. Initially, the β-ketoester is activated using the PDAN-Ni@Fe₃O₄ catalyst. Next, hydroxylamine hydrochloride attacks the C=O of the β-ketoester, then by eliminating one water the intermediate (II) is produced. The reaction is developed via the activation of II in the existence of -NH₂ groups in PDAN-Ni@Fe₃O₄. As a nucleophile, the Ni, Lewis acid site in isoxazole-5(4H)-ones attacks the C=O of the aldehyde to generate IV, then by eliminating one water the intermediate (V) is produced. The product (VII) was achieved through intramolecular *O*-attack cyclization.

The process parameters and outputs for the isoxazole 5(4H) compounds synthesis were compared with those of other catalysts described in the literature (Table 4). In this regard, we selected the reaction of 4-methoxybenzaldehyde, β-ketoester, and hydroxylamine hydrochloride, for the synthesis of 4i as a model. The findings show that our technique has quicker reaction times and produces greater production values. The multifunctional PDAN-Ni@Fe₃O₄ nanocomposite with active positions e.g., base (-NH₂ in PDAN backbone) and Lewis acid site (Fe³⁺ in Fe₃O₄ and Ni) play a noteworthy role in all stages of the reaction.

An attempt towards 1,4-Michael addition of pyrazolones to isoxazoles: Pyrazolones have been used as suitable nucleophiles in the preparation of heterocyclic. The aim of this part of the project was the 1,4-Michael addition of pyrazolones to isoxazoles. For this purpose, examined was the condensation of 3-methyl-1-phenyl-1H-pyrazole-5-ol and isoxazole-5(4H)-ones in ethanol in the existence of PDAN-Ni@Fe₃O₄ nanocomposite in a catalytic quantity. A range of temperatures, including 25, 40, 60, and 80 °C, were used. The model reaction was then conducted in the presence of PDAN-Ni@Fe₃O₄ in a catalytic quantity in several polar solvents, e.g., water, ethanol, water/ethanol (50:50), and solvent-free conditions. From the reactivity of the stated materials, in this condensation reaction, we expected the 1,4-Michael addition of pyrazolone to isoxazole to be the chief product. However, spectral studies have shown that the main product is bis-pyrazolone with a lower yield. In the ¹H NMR spectrum of 4,4-(aryl methylene)-bis(3-methyl-1-phenylpyrazol-5-ol) (Fig. 9) the signal at δ = 2.31 ppm (s, 6H) was owing to the methyl group on the pyrazolone rings, the protons of -OMe group seemed at δ = 3.67 ppm (s, 3H), the signal at δ = 4.85 ppm (s, 6H) was due to the benzylic proton. Also, protons of the aromatic unit appeared in the region of δ = 6.69–7.72 ppm (9H). The signals at δ = 8.76 and δ = 8.76 ppm were attributable to the O-H protons in the pyrazolone rings and aromatic unit.

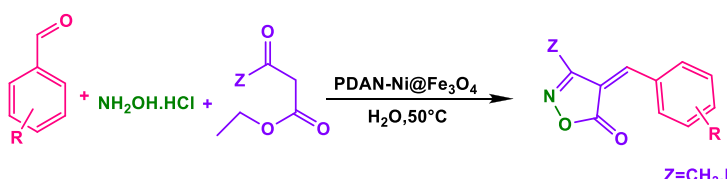
The reaction steps of the Michael addition of pyrazolone to isoxazole 5(4H) ones and finally preparing bis-pyrazolone are shown in Fig. 10.

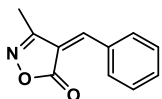
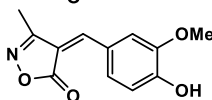
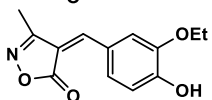
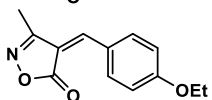
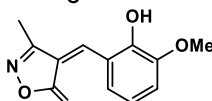
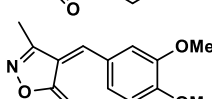
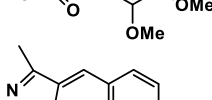
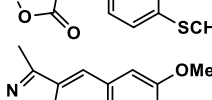
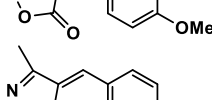
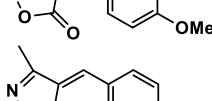
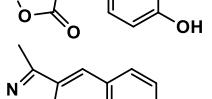
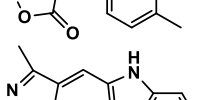
After the nucleophilic addition of pyrazolone to the isoxazole, the resulting intermediate (a) lost an isoxazole moiety due to the instability, and the intermediate (b) was formed. The intermediate (b) is rapidly attacked by another pyrazole nucleophile to produce bis-pyrazolone as the final product. All attempts for the recovery of intermediate (a) as the final product failed, because this intermediate was converted rapidly to intermediate (b) and then to the final bis-pyrazolone.

It was expected the isoxazole (4a) is activated using the PDAN-Ni@Fe₃O₄ and that the activation of isoxazole (4a) as a Michael receiver allows for the continuation of the reaction. Michael then added 3-methyl-1-phenyl-1H-pyrazol-5-ol, which resulted in intermediate (4 b), but the reaction did not go as planned (Fig. 10).

Based on the structure of the final product, in the case of isoxazole (4a) the equivalence of pyrazole was increased to two, which resulted in the production of bis-pyrazolone at a high yield. The effectiveness of this approach was checked by using another isoxazole (4 b, 4c, 4 d, 4f, 4 h, 4i, 4j, and 4q) the resulting bis pyrazolone obtained high yields.

Recovery: The reusing feasibility and recovery of PDAN-Ni@Fe₃O₄ for the creation of isoxazole-5(4H)-ones were examined. The PDAN-Ni@Fe₃O₄ was recycled after performing the reaction. The first PDAN-Ni@Fe₃O₄ catalyst was collected by a magnet and washed

Table 3Benzaldehyde derivatives conversion to isoxazole-5(4*H*)-ones in the existence of PDAN-Ni@Fe₃O₄.


Entry	Product ^b	code	Time (min)	Yield % ^b	M.P (°C)		Ref.
					Observed	Reported	
1		4a	60	90	140–142	140–142	[43]
2		4 b	25	95	214–216	211–214	[43]
3		4c	35	92	133–135	135–138	[44]
4		4 d	40	96	140–142	139–140	[44]
5		4e	30	96	108–110	108–109	[44]
6		4f	25	92	265–267	267–270	[43]
7		4 g	45	95	171–173		
8		4 h	30	93	135–137	135–136	[45]
9		4i	40	96	174–176	175–177	[43]
10		4j	25	92	212–214	214–216	[43]
11		4 k	30	90	135–137	135–136	[43]
12		4 l	60	93	241–243	242–244	[45]

(continued on next page)

Table 3 (continued)

Entry	Product ^b	code	Time (min)	Yield % ^b	M.P (°C)		Ref.
					Observed	Reported	
13		4 m	80	90	174–176	173–174	[46]
14		4n	20	96	226–228	227–228	[43]
15		4o	60	91	202–204	202–203	[43]
16		4p	65	90	144–145	145–146	[45]
17		4q	50	92	146–148	146–147	[43]
18		4r	60	93	238–239	227–229	[46]
		4s	30	95	88–90		
		4t	60	90	174–176		
19		4u	35	92	159–161	161–162	[44]
20		4v	30	93	214–216	213–215	[44]

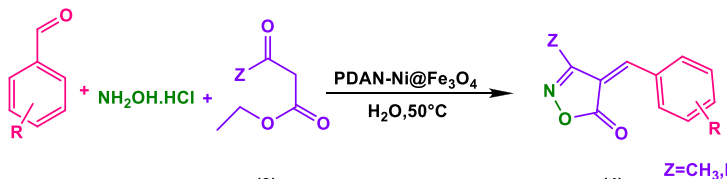
(continued on next page)

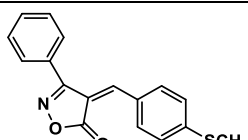
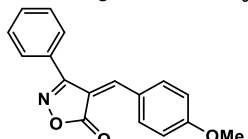
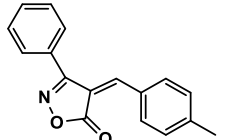
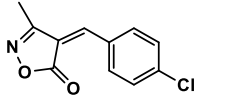
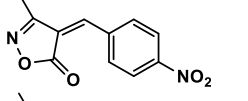
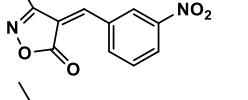
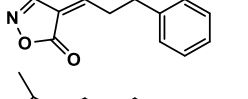
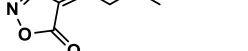
Table 3 (continued)

Entry	Product ^b	code	Time (min)	Yield % ^b	M.P (°C)		Ref.
					Observed	Reported	
21		4w	75	95	225–227	228–226	[47]
22		4x	80	94	211–212	212–215	[44]
23		4 y	40	96	149–151	150–152	[44]
24		4z	45	91	119–121	118–120	[44]
25		4aa	35	95	130–131		
26		4 ab	30	96	162–164	168–169	[44]
27		4ac	25	91	196–198	194–196	[47]
28		4ad	40	90	168–170	168–170	[17]

(continued on next page)

Table 3 (continued)



Entry	Product ^b	code	Time (min)	Yield % ^b	M.P (°C)		Ref.
					Observed	Reported	
29		4ae	45	92	184–186		
30		4af	40	90	167–169	168–169	[47]
31		4 ag	50	91	195–198	189–191	[47]
32		4ah	120	Not detected			
33		4ai	120	Not detected			
34		4aj	120	Not detected			
35		4ak	120	Not detected			
36		4 al	120	Not detected			

a Reaction conditions: aldehyde (1 mmol), β -ketoester (1 mmol), hydroxylamine hydrochloride (1 mmol), 5 mL water, and PDAN-Ni@Fe₃O₄ (0.04 g) at 50 °C.

^b Isolated yield.

with 5 mL of EtOH and dried in an oven (Fig. 11A). Afterward, the PDAN-Ni@Fe₃O₄ catalyst was used five consecutive times (Fig. 11B).

To prove the stability of the catalyst after recovery, the FTIR spectrum was taken from the PDAN-Ni@Fe₃O₄ nanocatalyst (Fig. 11C). As seen in the FTIR spectrum, very few changes in the characteristic peaks of the nanocatalyst indicate the stability of the nanocatalyst.

Antioxidant activity: The 2,2-diphenyl-1-picrylhydrazyl (DPPH) was applied to study the antioxidant property of PDAN, PDAN-Ni, PDAN-Ni@Fe₃O₄, and synthesized isoxazole-5(4H)-ones (Fig. 12) [52]. The antioxidant activity of all materials employed to make magnetic nanocatalysts ranged from 45 to 75%, according to the findings. Additionally, The antioxidant activity of 11 synthesized isoxazole-5(4H)-ones was investigated. Results showed that isoxazole-5(4H)-ones had antioxidant activities between 73% and 92%.

It seems the existence of –NH₂ groups in the PDAN and hydroxyl in the iron oxide nanoparticles is a logical reason for the higher antioxidant activity of PDAN-Ni@Fe₃O₄ than PDAN and PDAN-Ni. On the other hand, the existence of nitrogen in the isoxazole

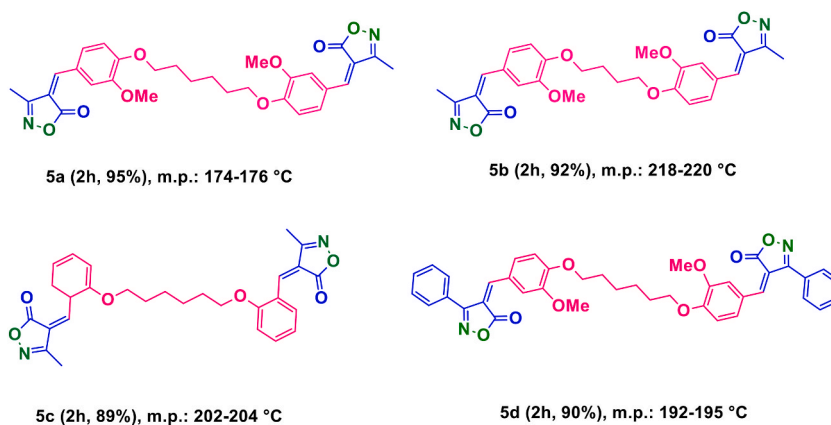


Fig. 7. Some new alkylene bridging bis 4-benzylidene-3-methyl isoxazole-5(4H)-ones. 5a: (4,4')-4,4'-(((hexane-1,6-diylbis (oxy)))bis (3-methoxy-4,1-phenylene))bis meth aneyl ylidene))bis (3-methylisoxazol-5(4H)-on; 5b: (4,4')-4,4'-(((hexane-1,4-diylbis (oxy)))bis (3-methoxy-4,1-phenylene)-)bis meth aneyl ylidene))bis (3-methylisoxazol-5(4H)-on; 5c: 3-methyl-4-(2-(((6-(((3-methyl-5-oxoisoxazol-4(5H)-ylidene)methyl)cyclohexa-1,3-dien-1-yl)oxy)hexyl)oxy)benzylidene)isoxazol-5(4H)-one; 5d: (4,4')-4,4'-(((hexane-1,6-diylbis (oxy)))bis (3-methoxy-4,1-phenylene))bis (methaneylylidene)) bis(3-phenylisoxazol-5(4H)-one).

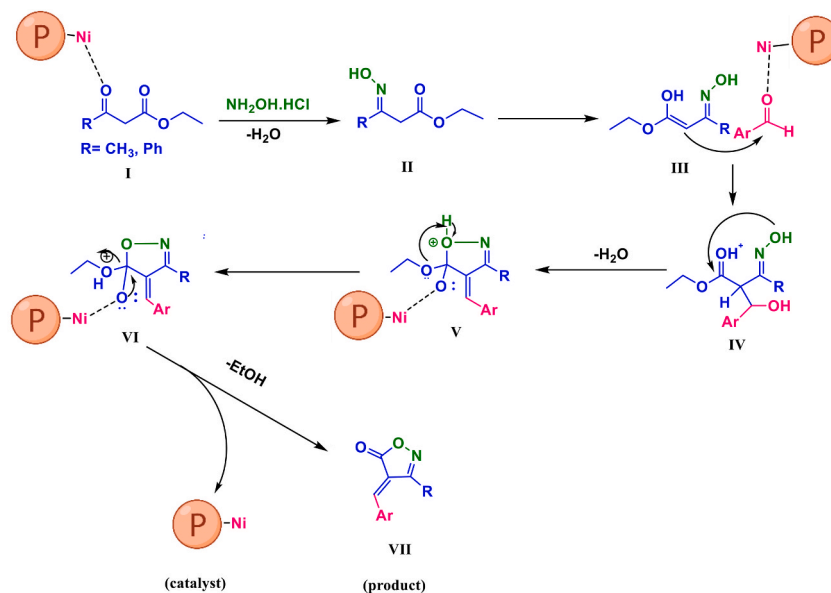


Fig. 8. Suggested mechanism scheme for the preparation of isoxazole-5(4H)-ones by PDAN-Ni@Fe₃O₄.

Table 4

Evaluating the catalytic efficiency of PDAN-Ni@Fe₃O₄ in comparison to other known catalysts for the manufacture of the 4i derivative.

Entry	Catalyst	Condition	Yield (%)	Time (Min.)	Ref.
1	PDAN-Ni@Fe ₃ O ₄ (0.04 g)	H ₂ O/50 °C	96	40	This study
2	Ni(OAc) ₂ H ₂ O	H ₂ O/R.T.	95	75	[48]
3	Sulfonated graphene-Oxide	Neat/R.T.	89	90	[49]
4	Phosphoric acid-based molten salt	H ₂ O/70 °C	90	85	[50]
5	Ag/SiO ₂	H ₂ O/R.T.	90	60	[42]
6	Fe ₃ O ₄ @MAP-SO ₃ H nanoparticles	H ₂ O/R.T.	90	120	[51]

R.T., room temperature.

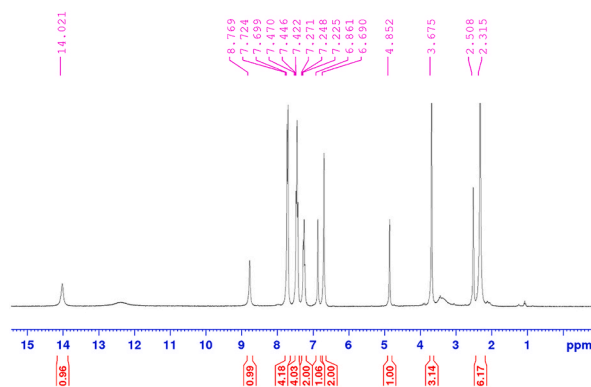


Fig. 9. ^1H NMR spectrum of 4,4-(arylmethylene)-bis(3-methyl-1-phenylpyrazol-5-ol).

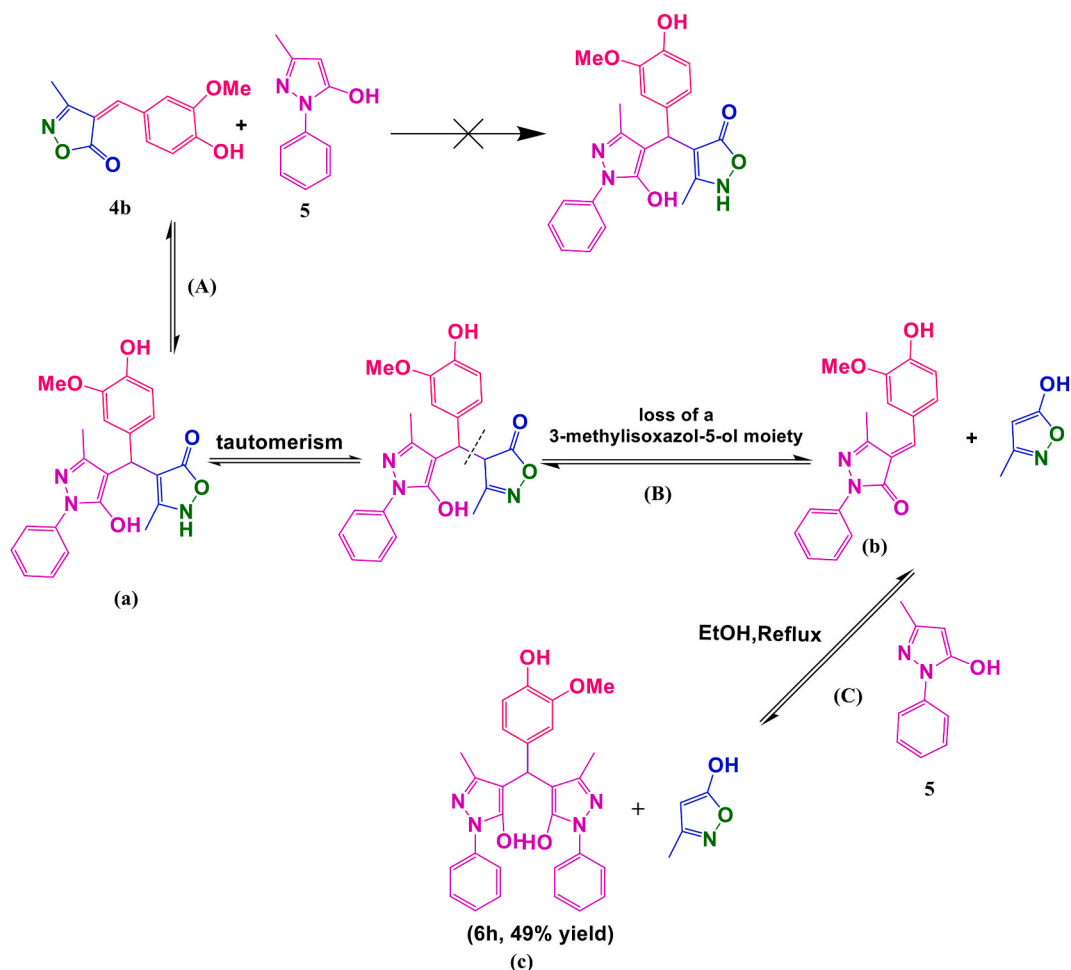


Fig. 10. Michael's addition of 3-methyl-1-phenyl-3-methyl-5-pyrazolone to isoxazole-5(4H)-ones.

derivatives leads to antioxidant activity.

Antibacterial activity: The antibacterial properties of Fe_3O_4 nanoparticles, PDAN, and isoxazole-5(4H)-ones (4c, 4d, 4f, 4g, 4j, 4n, 4s, and 4t) versus *Escherichia coli* and *Staphylococcus aureus* were examined *in vitro*, with the findings given in Fig. 13 and Table 5. The Fe_3O_4 nanoparticles were most effective against both species, but the PDAN was solely effective against *Escherichia coli*. Furthermore, the isoxazole-5(4H)-ones presented good activity versus *Staphylococcus aureus* than *Escherichia coli*.

4c: 3-Methyl-4-(4-Ethoxybenzylidene) isoxazole-5 (4H)-one; 4d: 3-Methyl-4-(4-ethoxy benzylidene) isoxazole-5 (4H)-one; 4f: 3-Methyl-4-(3,4,5-trimethoxybenzylidene) isoxazole-5 (4H)-one; 4g: 3-Methyl-4-(4-(methylthio)benzylidene) isoxazole-5 (4H)-one;

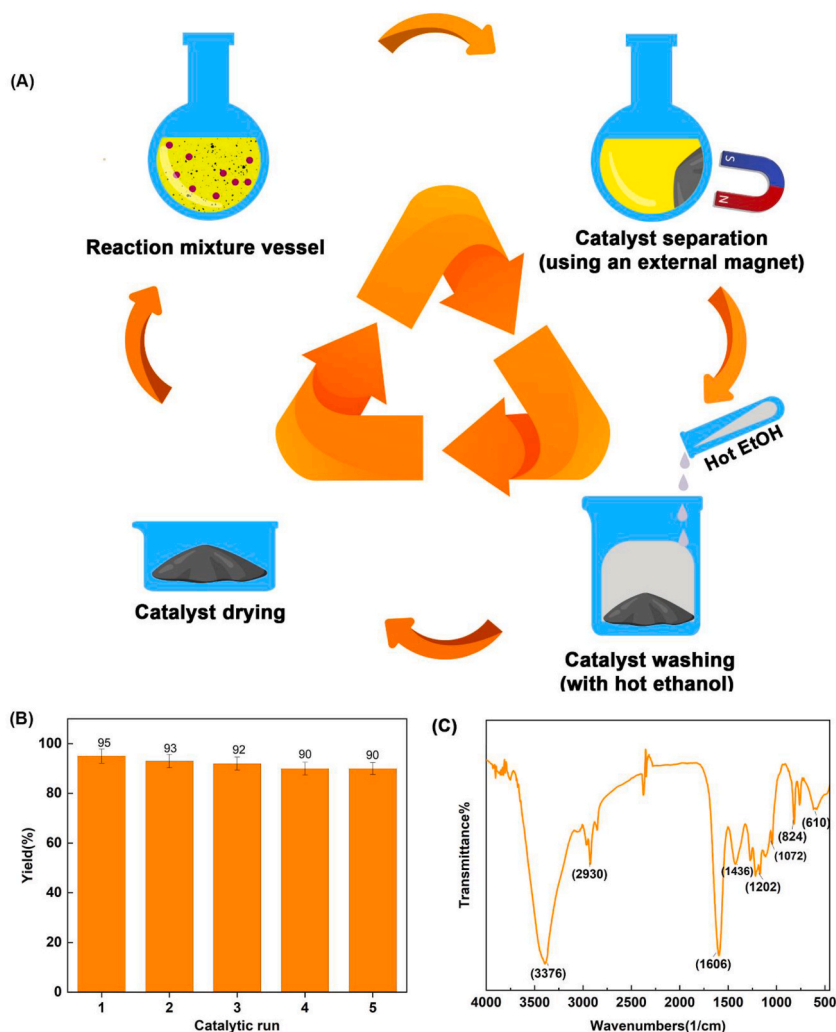


Fig. 11. Recovery cycle of the PDAN-Ni@Fe₃O₄ nanocatalyst (A), reusability of PDAN-Ni@Fe₃O₄ in the synthesis isoxazole-5(4H)-ones (B), and the FTIR spectrum of PDAN-Ni@Fe₃O₄ after recovery (C).

4j: 3-Methyl-4-(4-hydroxy benzylidene) isoxazole-5 (4H)-one; 4n: 3-Methyl-4-(4-(dimethylamino)benzylidene)isoxazole-5(4H)-one; 4t: 4-(naphthalen-1-ylmethylene)-3-phenylisoxazol-5(4H)-one; 4s: 3-methyl-4-(4-ethylbenzylidene)isoxazol-5(4H)-one.

4. Conclusions

A magnetic poly (1,8-diaminonaphthalene)-nickel complex nanocatalyst was synthesized from a combination of PDAN-Ni and Fe₃O₄ nanoparticles in three stages and applied in the synthesis of isoxazole-5(4H)-ones. The XRD and FESEM analyses showed that the magnetic catalyst had an amorphous nature. PDAN-Ni and PDAN-Ni@Fe₃O₄ were shown the high thermal stability than PDAN. The greatest yield of the isoxazole-5(4H)ones was 96% in 20 min with 0.06 g of catalyst in moderate conditions. At least five times of use could be made of the magnetic catalyst before it started to severely lose its catalytic activity. The nanocatalyst and isoxazole-5(4H)-ones showed antioxidant activity at 75% and 92%, respectively. Additionally, the nanocatalyst and isoxazole-5(4H)-ones were extremely active versus *Staphylococcus aureus* and *Escherichia coli*.

4.1. Spectroscopic data

3-Methyl-4-(4-Ethoxybenzylidene) isoxazole-5 (4H)-one (4c, Figure S1, S2): Solid, m. p.: 133–135 °C; FT-IR (KBr) $\nu_{\max}/\text{cm}^{-1}$: 3125, 2989, 1736, 1632, 1115, ¹H NMR (400 MHz, DMSO-*d*₆): δ (ppm) 1.38 (t, 3H, *J* = 6.8 Hz, CH₃), 2.24 (s, 3H, CH₃), 4.10 (q, 2H, *J* = 7.2 Hz, OCH₂), 6.97 (d, 2H, *J* = 8.4 Hz, aromatic), 7.76 (s, 1H, vinyl), 7.87 (dd, 1H, *J* = 8.4, 2 Hz), 8.51 (d, 1H, *J* = 2 Hz, aromatic), 10.74 (s, 1H, OH) ppm, ¹³C NMR (100 MHz, DMSO-*d*₆): δ = 11.76, 15.03, 64.26, 114.07, 116.30, 118.01, 125.53, 132.03, 147.10,

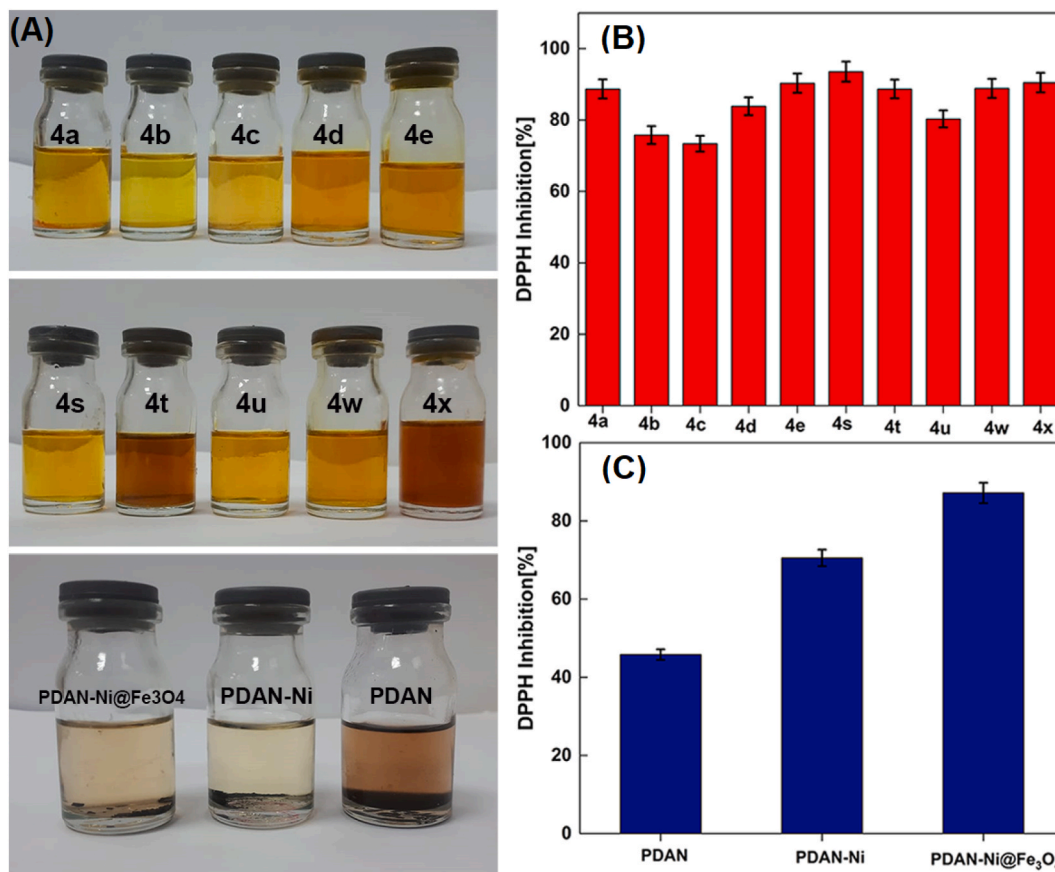


Fig. 12. The pictures (A) and bar charts of antioxidant activity (B and C) of isoxazole-5(4H)-ones derivatives and PDAN, PDAN-Ni, PDAN-Ni@Fe₃O₄. 4a: 3-methyl-4-benzylidene-isoxazol-5(4H)-one; 4b: 3-methyl-4-(4-hydroxy-3-methoxybenzylidene)isoxazol-5(4H)-one; 4c: 3-Methyl-4-(4-Ethoxybenzylidene) isoxazole-5 (4H)-one; 4d: 3-Methyl-4-(4-ethoxy benzylidene) isoxazole-5 (4H)-one; 4e: 3-Methyl-4-(2-hydroxy-3-methoxybenzylidene)isoxazol-5(4H)-one; 4s: 3-methyl-4-(4-ethylbenzylidene)isoxazol-5(4H)-one; 4t, 4-(naphthalen-1-ylmethylene)-3-phenylisoxazol-5(4H)-one; 4u: 3-phenyl-4-(3,4-dihydroxybenzylidene)isoxazol-5(4H)-one; 4w: 3-(Phenyl)-4-((thiophen-2-yl)methylene)isoxazole-5(4H)-one; 4x: 3-(Phenyl)-4-(1H-indol-3-yl)methylene)-isoxazole-5(4H)-one.

152.40, 154.50, 162.75, 169.49 ppm.

3-Methyl-4-(4-ethoxy benzylidene) isoxazole-5 (4H)-one (4d, Figure S3, S4): Solid, m. p.: 140–142 °C; FT-IR (KBr) $\nu_{\max}/\text{cm}^{-1}$: 3123, 2991, 1734, 1630, 1112; ¹H NMR (400 MHz, DMSO-*d*₆): δ (ppm) 1.36 (t, 3H, *J* = 6.8 Hz, CH₃), 2.26 (s, 3H, CH₃), 4.10 (q, 2H, *J* = 6.8 Hz, OCH₂), 7.14 (d, 2H, *J* = 8.8 Hz, aromatic), 7.86 (s, 1H, vinyl), 8.52 (d, 2H, *J* = 8.8 Hz) ppm, ¹³C NMR (100 MHz, DMSO-*d*₆): δ = 11.78, 14.90, 64.44, 115.49, 115.52, 126.15, 137.47, 151.76, 162.77, 164.09, 169.12 ppm.

3-Methyl-4-(3,4,5-trimethoxybenzylidene) isoxazole-5 (4H)-one (4f, Figure S5, S6): Solid, m. p.: 265–267 °C; FT-IR (KBr) $\nu_{\max}/\text{cm}^{-1}$: 3136, 2987, 1739, 1643, 1128; ¹H NMR (DMSO-*d*₆, 400 MHz): δ (ppm) 2.26 (s, 3H, CH₃), 3.83 (s, 6H, OCH₃), 3.90 (s, 3H, OCH₃), 7.20 (d, 1H, *J* = 8.4 Hz, aromatic) 7.21 (s, 1H, vinyl), 8.01 (dd, 1H, *J* = 8.8 Hz, 2. Hz aromatic), 8.50 (d, 1H, *J* = 1.6 Hz, aromatic) ppm, ¹³C NMR (100 MHz, DMSO-*d*₆): δ = 11.78, 55.92, 56.45, 112.08, 115.49, 115.95, 126.50, 131.54, 148.79, 152.21, 154.84, 162.78, 169.27 ppm.

3-Methyl-4-(4-(methylthio)benzylidene) isoxazole-5 (4H)-one (4g, Figure S7, S8): Solid, m. p.: 171–173 °C; FT-IR (KBr) $\nu_{\max}/\text{cm}^{-1}$: 3125, 2965, 1742, 1644, 1123; ¹H NMR (400 MHz, DMSO-*d*₆): δ (ppm) = 2.27 (s, 3H, CH₃), 3.35 (s, 3H, SCH₃), 7.45 (d, 2H, *J* = 8.8 Hz, aromatic), 7.88 (s, 1H, vinyl), 8.41 (d, 2H, *J* = 8.8 Hz, aromatic) ppm, ¹³C NMR (100 MHz, DMSO-*d*₆): δ = 11.79, 14.26, 117.32, 125.36, 129.28, 134.67, 148.50, 151.44, 162.73, 168.82 ppm.

3-Methyl-4-(3,4-dimethoxy benzylidene) isoxazole-5 (4H)-one (4h, Figure S9, S10): Solid, m. p.: 135–137 °C; FT-IR (KBr) $\nu_{\max}/\text{cm}^{-1}$: 3121, 2971, 1737, 1641, 1121; ¹H NMR (400 MHz, DMSO-*d*₆): δ (ppm) = 2.27 (s, 3H, CH₃), 3.84 (s, 3H, OCH₃), 3.91 (s, 3H, OCH₃), 7.21 (d, 1H, *J* = 8.8 Hz, aromatic), 7.86 (s, 1H, vinyl), 8.02 (d, 1H, *J* = 8.4 Hz, aromatic), 8.50 (d, 1H, *J* = 1.6 Hz, aromatic) ppm, ¹³C NMR (100 MHz, DMSO-*d*₆): δ = 11.78, 55.93, 56.45, 112.09, 115.50, 115.97, 126.50, 131.54, 148.80, 152.23, 154.84, 162.78, 169.27 ppm.

3-Methyl-4-(4-hydroxy benzylidene) isoxazole-5 (4H)-one (4j, Figure S11, S12): Solid, m. p.: 212–214 °C; FT-IR (KBr) $\nu_{\max}/\text{cm}^{-1}$: 3126, 2976, 1739, 1645, 1124; ¹H NMR (400 MHz, DMSO-*d*₆): δ (ppm) = 2.40 (s, 3H, CH₃), 6.96 (d, 2H, *J* = 8.8 Hz, aromatic), 7.77 (s, 1H, vinyl), 8.44 (d, 2H, *J* = 8.8 Hz, aromatic), 11.13 (s, 1H, OH) ppm, ¹³C NMR (100 MHz, DMSO-*d*₆): δ = 11.76, 114.25,

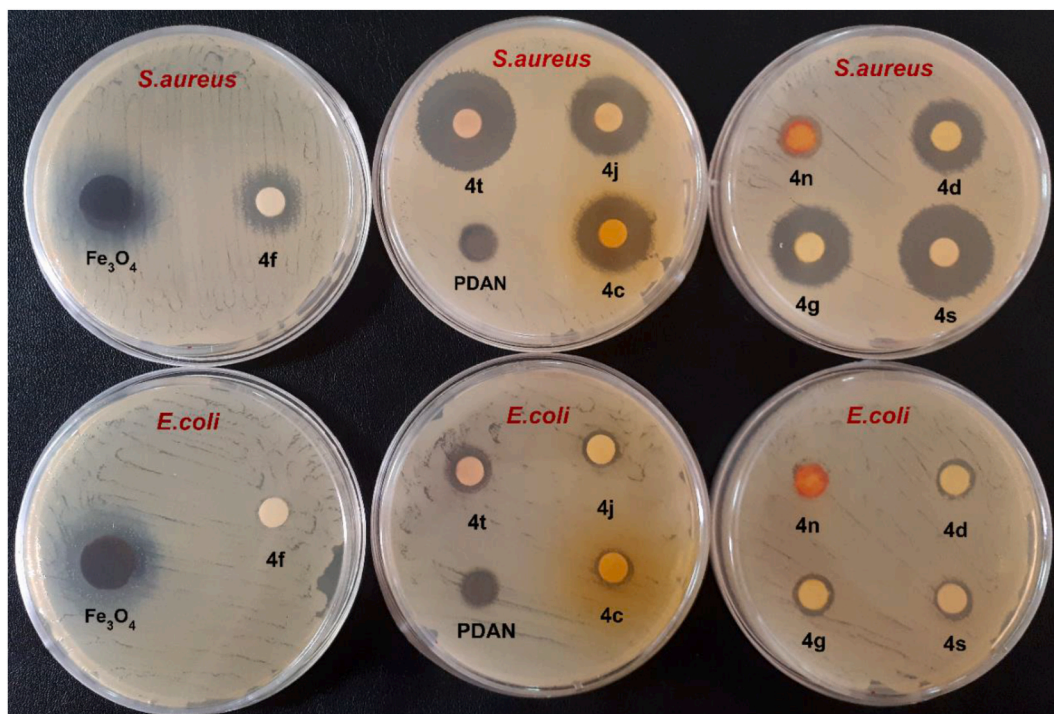


Fig. 13. Antibacterial activities of the Fe_3O_4 nanoparticles, PDAN, and some isoxazole-5(4H)-ones versus *Escherichia coli* and *Staphylococcus aureus*. 4c: 3-Methyl-4-(4-Ethoxybenzylidene) isoxazole-5 (4H)-one; 4d: 3-Methyl-4-(4-ethoxy benzylidene) isoxazole-5 (4H)-one; 4f: 3-Methyl-4-(3,4,5-trimethoxybenzylidene) isoxazole-5 (4H)-one; 4g: 3-Methyl-4-(4-(methylthio)benzylidene) isoxazole-5 (4H)-one; 4j: 3-Methyl-4-(4-hydroxy benzylidene) isoxazole-5 (4H)-one; 4n: 3-Methyl-4-(4-(dimethylamino)benzylidene)isoxazole-5(4H)-one; 4t:4-(naphthalen-1-ylmethylene)-3-phenylisoxazol-5(4H)-one; 4s: 3-methyl-4-(4-ethylbenzylidene)isoxazol-5(4H)-one.

Table 5

Antibacterial activities of the Fe_3O_4 nanoparticles, PDAN, and some isoxazole-5(4H)-ones versus *Escherichia coli* and *Staphylococcus aureus*.

Entry	Compound	Inhibition Zone (mm)	
		<i>Staphylococcus aureus</i> Gram-Positive (+)	<i>Escherichia coli</i> Gram-Negative (-)
1	Fe_3O_4 NPs	27 ± 02	24 ± 02
2	PDAN	10 ± 01	10 ± 05
3	4c	19 ± 0.6	10 ± 07
4	4 d	20 ± 0.7	11 ± 1.2
5	4f	16 ± 1.0	9 ± 05
6	4 g	21 ± 1.0	11 ± 02
7	4j	20 ± 1.0	10 ± 0.2
8	4n	12 ± 1.0	NE ^a
9	4s	24 ± 0.7	11
10	4t	25 ± 02	12 ± 05
11	Gentamicin	26 ± 1.2	19.6 ± 0.7
12	Chloramphenicol	22.3 ± 1.7	20.7 ± 1.0

^a No effect.

116.63, 125.01, 138.00, 152.00, 162.74, 164.41, 169.31 ppm.

4-((1H-indol-3-yl)methylene)-3-methylisoxazole-5(4H)-one (4l, Figure S13, S14) Solid, m. p.: 241–243 °C; FT-IR (KBr) $\nu_{\text{max}}/\text{cm}^{-1}$: 3434.3115, 2989, 1738, 1629, 1126; ^1H NMR (300 MHz, $\text{DMSO}-d_6$): δ (ppm) = 2.31 (s, 3H, CH_3), 8.12 (s, 1H, vinyl), 9.51 (s, 1H, aromatic), 7.30–7.36 (m, 2H, aromatic), 7.58–7.63 (m, 2H, aromatic), 12.80 (s, NH). ^{13}C NMR (100 MHz, $\text{DMSO}-d_6$): δ = 11.65, 108.30, 112.14, 114.57, 118.24, 123.00, 124.17, 136.84, 138.95, 141.75 ppm.

3-Methyl-4-(3-phenylallylidene)isoxazole-5(4H)-one (4m, Figure S15): Solid, m. p.: 174–176 °C; FT-IR (KBr) $\nu_{\text{max}}/\text{cm}^{-1}$: 3127, 2991, 1739, 1646, 1139; ^1H NMR (300 MHz, $\text{DMSO}-d_6$): δ (ppm) 2.34 (s, 3H), 7.49–7.51 (m, 4H), 7.68–7.84 (m, 4H), 8.09–8.18 (m, 1H).

3-Methyl-4-(4-(dimethylamino)benzylidene)isoxazole-5(4H)-one(4n, Figure S16, S17): Solid, m. p.: 226–228 °C; FT-IR (KBr) $\nu_{\text{max}}/\text{cm}^{-1}$: 3129, 2976, 1731, 1651, 1125; ^1H NMR (400 MHz, $\text{DMSO}-d_6$): δ (ppm) = 2.21 (s, 3H, CH_3), 3.84 (s, 6H, $\text{N}(\text{CH}_3)_2$), 6.86 (d, 2H, J = 9.9 Hz, aromatic), 7.6.2 (s, 1H, vinyl), 8.46 (d, 2H, J = 8.4 Hz, aromatic) ppm, ^{13}C NMR (100 MHz, $\text{DMSO}-d_6$): δ = 11.81,

109.44, 112.11, 121.46, 138.05, 150.98, 154.82, 162.62, 170.39 ppm.

3-Methyl-4-(2-hydroxybenzylidene)isoxazole-5(4H)-one (4o, Figure S18, S19): Solid, m. p.: 202–204 °C; FT-IR (KBr) $\nu_{\max}/\text{cm}^{-1}$: 3129, 2969, 1744, 1633, 1119; ^1H NMR (400 MHz, DMSO- d_6): δ (ppm) = 2.26 (s, 3H, CH₃), 6.93 (t, 1H, J = 7.2 Hz, aromatic), 7.01 (d, 1H, J = 8.4 Hz, aromatic), 7.49 (td, 1H, J = 8 Hz, 2 Hz, aromatic), 8.09 (s, 1H, vinyl), 8.74 (dd, 1H, J = 8 Hz, 1.6 Hz aromatic), 11.02 (s, 1H, OH) ppm, ^{13}C NMR (100 MHz, DMSO- d_6): δ = 11.69, 111.60, 116.89, 119.57, 119.93, 132.78, 137.24, 145.48, 160.12, 162.64, 168.75 ppm.

3-methyl-4-(thiophen-2-ylmethylene)isoxazole-5(4H)-one (4p, Figure S20, S21): Solid, m. p.: 144–145 °C; FT-IR (KBr) $\nu_{\max}/\text{cm}^{-1}$: 3120, 2981, 1735, 1625, 1118; ^1H NMR (400 MHz, DMSO- d_6): δ (ppm) = 2.26 (s, 3H, CH₃), 7.39 (t, 1H, J = 3.6 Hz, aromatic), 8.22 (dd, 1H, J = 4 Hz, 0.8 Hz aromatic), 8.26 (s, 1H, vinyl), 8.32 (d, 1H, J = 4.8 Hz) ppm, ^{13}C NMR (100 MHz, DMSO- d_6): δ = 11.59, 113.48, 129.47, 136.66, 141.70, 142.11, 143.60, 162.13, 169.00 ppm.

3-Methyl-4-(2-methoxybenzylidene)isoxazole-5(4H)-one (4q, Figure S22, S23): Solid, m. p.: 146–148 °C; FT-IR (KBr) $\nu_{\max}/\text{cm}^{-1}$: 3128, 2966, 1721, 1639, 1116; ^1H NMR (400 MHz, DMSO- d_6): δ (ppm) = 2.26 (s, 3H, CH₃), 3.93 (s, 3H, OCH₃), 7.09 (t, 1H, J = 7.6 Hz, aromatic), 7.20 (d, 1H, J = 8.4 Hz, aromatic), 7.65 (td, 1H, J = 7.6 Hz, 1.6 Hz aromatic), 8.06 (s, 1H, vinyl), 8.63 (dd, 1H, J = 8 Hz, 1.6 Hz aromatic) ppm, ^{13}C NMR (100 MHz, DMSO- d_6): δ = 11.67, 15.16, 56.67, 112.23, 118.35, 120.71, 120.93, 132.78, 136.94, 145.19, 160.07, 162.48, 168.36 ppm.

4-(naphthalen-1-ylmethylene)-3-phenylisoxazol-5(4H)-one (4t, Figure S24, S25): Solid, m. p.: 174–176 °C; FT-IR (KBr) $\nu_{\max}/\text{cm}^{-1}$: 3128, 2966, 1721, 1639, 1116; ^1H NMR (400 MHz, DMSO- d_6): δ (ppm) = 7.08 (d, 1H, J = 4.8 Hz, aromatic), 7.62–7.70 (m, 5H, aromatic), 7.83–7.85 (m, 2H, aromatic), 7.96–7.99 (m, 1H, aromatic), 8.05–8.08 (m, 1H, aromatic), 8.22 (d, 1H, J = 8.4 Hz, aromatic), 8.48 (d, 1H, J = 7.6 Hz, aromatic), 8.60 (s, 1H, aromatic) ppm, ^{13}C NMR (100 MHz, DMSO- d_6): δ = 119.95, 124.32, 125.52, 127.20, 127.58, 128.24, 128.27, 128.45, 128.56, 129.17, 129.47, 129.84, 131.65, 131.68, 133.39, 134.16, 149.75, 150.79, 162.18, 163.74, 168.02.

3-(Phenyl)-4-(4-hydroxy-3-ethoxy benzylidene)-3-methylisoxazol-5(4H)-one (4v, Figure S26, S27): Solid, m. p.: 214–216 °C; FT-IR (KBr) $\nu_{\max}/\text{cm}^{-1}$: 3410, 3125, 1724, 1622, 1154; ^1H NMR (300 MHz, DMSO- d_6): δ (ppm) = 3.86 (s, 3H, CH₃), 6.95 (d, 1H, J = 8.4, aromatic), 7.75–7.67 (m, 6H, aromatic), 7.90 (d, 1H, J = 6.6 Hz, aromatic), 8.49 (s, 1H, vinyl), 10.90 (s, 1H, OH). ^{13}C NMR (75 MHz, DMSO- d_6): δ = 56.17, 113.05, 116.26, 117.58, 125.49, 127.89, 129.39, 129.54, 131.19, 132.57, 147.85, 153.88, 154.86, 164.78, 169.42 ppm.

3-(Phenyl)-4-((thiophen-2-yl)methylene)isoxazole-5(4H)-one (4w, Figure S28, S29): Solid, m. p.: 225–227 °C; FT-IR (KBr) $\nu_{\max}/\text{cm}^{-1}$: 3125, 1736, 1643, 1129; ^1H NMR (300 MHz, DMSO- d_6): δ (ppm) = 7.40 (d, 1H, J = 3.9, aromatic), 7.63–7.74 (m, 5H, aromatic), 8.21 (d, J = 3.9 Hz, 1H, aromatic), 8.31 (t, 1H, J = 3.1 Hz, aromatic), 8.42 (s, 1H, vinyl). ^{13}C NMR (75 MHz, DMSO- d_6): δ = 112.12, 127.70, 129.12, 129.48, 129.72, 133.42, 136.70, 142.76, 142.78, 143.78, 145.23, 163.83, 169.33 ppm.

3-(Phenyl)-4-((1H-indol-3-yl)methylene)isoxazole-5(4H)-one (4x, Figure S30, S31): Solid, m. p.: 211–212 °C; FT-IR (KBr) $\nu_{\max}/\text{cm}^{-1}$: 3114, 1729, 1627, 1141; ^1H NMR (300 MHz, DMSO- d_6): δ (ppm) = 8.07 (s, 1H, vinyl), 9.61 (s, 1H, aromatic), 7.26–7.77 (m, 9H, aromatic), 12.95 (s, 1H, NH). ^{13}C NMR (75 MHz, DMSO- d_6): δ = 107.38, 113.32, 113.83, 117.63, 123.37, 124.73, 128.37, 128.79, 129.46, 129.75, 131.04, 137.02, 139.94, 141.63, 164.14, 171.04 ppm.

3-(Phenyl)-4-(4-ethyl benzylidene) isoxazole-5 (4H)-one (4z, Figure S32, S33): Solid, m. p.: 119–121 °C; FT-IR (KBr) $\nu_{\max}/\text{cm}^{-1}$: 3118, 2983, 1741, 1614; ^1H NMR (300 MHz, DMSO- d_6): δ (ppm) 1.21 (t, 3H, J = 7.5 Hz, CH₃), 2.70 (q, 2H, J = 7.8 Hz –CH₂), 7.41 (d, 2H, J = 8.4 Hz, aromatic), 7.62–7.72 (m, 5H, aromatic), 7.78 (s, 1H, vinyl), 8.33 (d, 2H, J = 8.1 Hz, aromatic). ^{13}C NMR (75 MHz, DMSO- d_6): δ = 15.47, 27.99, 117.26, 127.56, 127.93, 128.55, 128.65, 129.19, 129.24, 129.54, 129.70, 130.53, 130.55, 131.44, 133.41, 134.79, 151.90, 153.76, 164.51, 168.51 ppm.

3-(Phenyl)-4-(3,4,5-trimethoxybenzylidene)isoxazol-5(4H)-one (4 ab, Figure S34, S35): Solid, m. p.: 163–164 °C; FT-IR (KBr) $\nu_{\max}/\text{cm}^{-1}$: 3108, 1748, 1631, 1126; ^1H NMR (300 MHz, DMSO- d_6): δ (ppm) 3.85 (s, 9H, OCH₃), 7.99 (s, 2H, aromatic), 7.67–7.76 (m, 6H, aromatic). ^{13}C NMR (75 MHz, DMSO- d_6): δ = 55.68, 56.63, 60.69, 112.20, 112.84, 116.04, 116.46, 122.07, 127.62, 128.26, 128.63, 129.11, 129.38, 129.55, 129.69, 130.90, 131.38, 143.83, 152.11, 152.48, 152.75, 153.54, 161.50, 164.62, 168.80, 170.22 ppm.

(4,4')-4,4'-(((hexane-1,6-diylbis(oxy))bis(3-methoxy-4,1-phenylene))bis meth aneyl ylidene))bis(3-methylisoxazol-5(4H)-on (5a, Figure S36, S37) Yellow powder, m. p.: 174–176 °C; FT-IR (KBr) $\nu_{\max}/\text{cm}^{-1}$: 3120, 1728, 1620, 1112, ^1H NMR (300 MHz, DMSO- d_6): δ (ppm) 1.51 (br, 2H, CH₂, bridge), 1.81 (br, 2H, CH₂, bridge), 2.27 (s, 3H, CH₃), 3.84 (s, 3H, OCH₃), 4.12–4.16 (m, 2H, OCH₂, bridge), 7.16–7.21 (m, 1H, aromatic), 7.85–7.86 (m, 1H, aromatic), 7.99–8.04 (m, 1H, aromatic), 8.49 (s, 1H, H-Vinyl). ^{13}C NMR (75 MHz, DMSO- d_6): δ = 25.72, 25.82, 28.88, 55.99, 68.84, 114.29, 116.41, 118.23, 126.60, 129.94, 147.10, 152.42, 154.50, 162.76, 169.50, 191.84 ppm.

(4,4')-4,4'-(((hexane-1,4-diylbis(oxy))bis(3-methoxy-4,1-phenylene))bis meth aneyl ylidene))bis(3-methylisoxazol-5(4H)-on (5b, Figure S38, S39) Yellow powder, m. p.: 218–220 °C; FT-IR (KBr) $\nu_{\max}/\text{cm}^{-1}$: 3121, 1731, 1625, 1123, ^1H NMR (400 MHz, DMSO- d_6): δ (ppm) 1.93 (br, 2H, CH₂, bridge), 2.27 (s, 3H, CH₃), 3.84 (s, 3H, OCH₃), 4.20 (t, 2H, OCH₂, J = 6.4 Hz, bridge), 7.17–7.23 (m, 2H, aromatic), 7.39 (d, 1H, J = 1.6 Hz aromatic), 7.55 (dd, 1H, J = 8 Hz, 2 Hz aromatic), 8.86 (s, 1H, H-Vinyl). ^{13}C NMR (75 MHz, DMSO- d_6): δ = 11.77, 15.03, 62.36, 64.26, 114.09, 116.31, 118.03, 125.53, 123.03, 147.10, 152.42, 154.50, 162.76, 169.50 ppm.

3-methyl-4-2-(((6-((3-methyl-5-oxoisoxazol-4(5H)-ylidene)methyl)cyclohexa-1,3-dien-1-yl)oxy)hexyl)oxy)benzylidene)isoxazol-5(4H)-one (5c, Figure S40, S41) Yellow powder, m. p.: 202–204 °C; FT-IR (KBr) $\nu_{\max}/\text{cm}^{-1}$: 3117, 1733, 1627, 1125, ^1H NMR (400 MHz, DMSO- d_6): δ (ppm) 1.57 (br, 2H, CH₂, bridge), 1.85 (br, 2H, CH₂, bridge), 2.14 (s, 3H, CH₃), 4.16 (m, 2H, J = 6 Hz OCH₂, bridge), 7.04–7.10 (m, 1H, aromatic), 7.18–7.23 (m, 1H, aromatic), 7.60–7.67 (m, 1H, aromatic), 8.00 (s, 1H, H-Vinyl), 8.68 (d, 1H, J = 8 Hz, aromatic). ^{13}C NMR (75 MHz, DMSO- d_6): δ = 11.41, 25.62, 28.77, 68.83, 113.01, 113.13, 113.93, 120.76, 124.64,

128.07, 132.80, 136.93, 144.55, 159.67, 161.50, 162.39, 168.33, 189.57 ppm.

(4,4′)-4,4′-(((hexane-1,6-diylbis(oxy))bis(3-methoxy-4,1-phenylene))bis(methaneylylidene)) bis(3-phenylisoxazol-5 (4H)-one) (**5d**, [Figure S42](#), [S43](#)) Yellow powder, m. p.: 192–195 °C; FT-IR (KBr) $\nu_{\max}/\text{cm}^{-1}$: 3123, 1726, 1621, 1119 ^1H NMR (300 MHz, DMSO- d_6): δ (ppm) 1.49 (br, 2H, CH₂, bridge), 1.79 (br, 2H, CH₂, bridge), 3.99 (s, 3H, OCH₃), 4.13 (q, 2H, J = 6.8 Hz, OCH₂, bridge), 7.16–7.20 (m, 2H, aromatic), 7.60–7.64 (m, 5H, aromatic), 7.72 (s, 1H, H-Vinyl), 8.03–8.06 (m, 1H, aromatic). ^{13}C NMR (75 MHz, DMSO- d_6).

Author contribution statement

Shefa Mirani Nezhad: Performed the experiments; Wrote the paper.

Seied Ali Pourmousavi, Ehsan Nazarzadeh Zare: Conceived and designed the experiments; Analyzed and interpreted the data.

Golnaz Heidari, Samenesadat Hosseini, Mahla Peyvandtalab: Contributed reagents, materials, analysis tools or data.

Data availability statement

Data will be made available on request.

Additional information

Correspondence and requests for materials should be addressed to Ehsan Nazarzadeh Zare.

Declaration of competing interest

The authors declare that they have no known competing financial interests or personal relationships that could have appeared to influence the work reported in this paper.

Acknowledgments

The authors gratefully acknowledge the Vice-President's Office for the research affairs of Damghan University for supporting this project.

Appendix A. Supplementary data

Supplementary data to this article can be found online at <https://doi.org/10.1016/j.heliyon.2023.e15886>.

References

- [1] F. Hassanzadeh-Afruzi, A. Maleki, E.N. Zare, Novel eco-friendly acacia gum-grafted-polyamidoxime@copper ferrite nanocatalyst for synthesis of pyrazolopyridine derivatives, *J. Nanostruct. Chem.* (2022). <https://doi.org/10.1007/s40097-022-00471-8>.
- [2] M.R. Sarfjoo, A. Shad, M. Hassanpour, R. Varma, An overview on new anticancer drugs approved by food and drug administration: impending economic and environmental challenges, *Mater. Chem. Horizons* (2022), <https://doi.org/10.22128/mch.2022.588.1019>.
- [3] F. Heidarzadeh, E. Rahimi, Synthesis of 3-substituted indoles through yonemitsu reaction with copper benzene-1,3,5-tricarboxylate acid catalyst, *Mater. Chem. Horizons* (2022), <https://doi.org/10.22128/mch.2022.590.1021>.
- [4] P. Anastas, J. Warner, *Cover for Green Chemistry: Theory and Practice Green Chemistry: Theory and Practice*, Oxford University Press Inc, 1998.
- [5] A.N. Marzieh, M. Deinavizadeh, A.R. Kiasat, Fe₃O₄@SiO₂/DABCO(OH) core-shell hybrid nanocomposite: efficient nanomagnetic and basic reusable catalyst in the one-pot synthesis of trithiocarbonate derivatives, *Mater. Chem. Horizons* (2023), <https://doi.org/10.22128/mch.2023.634.1035>.
- [6] T. Bm, The atom economy—a search for synthetic efficiency, *Science* 80 (254) (1991) 1471–1477, <https://doi.org/10.1126/science.1962206>.
- [7] S. Barata-Vallejo, M.V. Cooke, A. Postigo, Radical fluoroalkylation reactions, *ACS Catal.* 8 (2018) 7287–7307.
- [8] J. Zhu, J. Mo, H. zhi Lin, Y. Chen, H. peng Sun, The recent progress of isoxazole in medicinal chemistry, *Bioorg. Med. Chem.* 26 (2018) 3065–3075, <https://doi.org/10.1016/j.bmc.2018.05.013>.
- [9] M.M.M. Santos, N. Faria, J. Iley, S.J. Coles, M.B. Hursthouse, M.L. Martins, R. Moreira, Reaction of naphthoquinones with substituted nitromethanes. Facile synthesis and antifungal activity of naphtho[2,3-d]isoxazole-4,9-diones, *Bioorg. Med. Chem. Lett* 20 (2010) 193–195, <https://doi.org/10.1016/j.bmcl.2009.10.137>.
- [10] M.M. Mojtahedi, M. Javadpour, M.S. Abaee, Convenient ultrasound mediated synthesis of substituted pyrazolones under solvent-free conditions, *Ultrason. Sonochem.* 15 (2008) 828–832, <https://doi.org/10.1016/j.ultsonch.2008.02.010>.
- [11] H. Kano, I. Adachi, R. Kido, K. Hirose, Isoxazoles. XVIII. Synthesis and pharmacological properties of 5-aminoalkyl- and 3-aminoalkylisoxazoles, *J. Org. Chem.* 553 (1967) 411.
- [12] A. Padmaja, C. Rajasekhar, A. Muralikrishna, V. Padmavathi, Synthesis and antioxidant activity of oxazolyl/thiazolylsulfonylemethyl pyrazoles and isoxazoles, *Eur. J. Med. Chem.* 46 (2011) 5034–5038, <https://doi.org/10.1016/j.ejmech.2011.08.010>.
- [13] P. Diana, A. Carbone, P. Barraja, G. Kelter, H.H. Fiebig, G. Cirrincione, Synthesis and antitumor activity of 2,5-bis(3'-indolyl)-furans and 3,5-bis(3'-indolyl)-isoxazoles, nortoposentin analogues, *Bioorg. Med. Chem.* 18 (2010) 4524–4529, <https://doi.org/10.1016/j.bmc.2010.04.061>.
- [14] T. Karabasanagouda, A.V. Adhikari, M. Girisha, Synthesis of some new pyrazolines and isoxazoles carrying 4-methylthiophenyl moiety as potential analgesic and antiinflammatory agents, *Indian J. Chem. B Org.* 48 (2009) 430–437.

- [15] D.B. Lowe, S. Magnuson, N. Qi, A.-M. Campbell, J. Cook, Z. Hong, M. Wang, M. Rodriguez, F. Acebe, H. Kluender, W.C. Wong, W.H. Bullock, A.I. Salhanick, T. Witman-Jones, M.E. Bowling, C. Keiper, K.B. Clairmont, In vitro SAR of (5-(2H)-isoxazolonyl) ureas, potent inhibitors of hormone-sensitive lipase, *Bioorg. Med. Chem. Lett.* 14 (2004) 3155–3159, <https://doi.org/10.1016/j.bmcl.2004.04.015>.
- [16] J.J. Donleavy, E.E. Gilbert, A synthesis of arylidene Isoxazolones1, *J. Am. Chem. Soc.* 59 (1937) 1072–1076, <https://doi.org/10.1021/ja01285a032>.
- [17] D. Villemin, B. Garrigues, Potassium fluoride on alumina: dry condensation of 3-phenylisoxazol-5-one with aldehydes under microwave irradiation, *Synth. Commun.* 23 (1993) 2251–2257, <https://doi.org/10.1080/00397919308013781>.
- [18] I. Nakamura, M. Okamoto, M. Terada, Gold-catalyzed cyclization and subsequent arylidene group transfer of O-propionyl oximes, *Org. Lett.* 12 (2010) 2453–2455, <https://doi.org/10.1021/ol100581m>.
- [19] K. Chanda, S. Rej, M.H. Huang, Investigation of facet effects on the catalytic activity of Cu2O nanocrystals for efficient regioselective synthesis of 3,5-disubstituted isoxazoles, *Nanoscale* 5 (2013) 12494–12501, <https://doi.org/10.1039/C3NR03790H>.
- [20] J. Li, S. Yang, W. Wu, H. Jiang, Recent advances in Pd-catalyzed cross-coupling reaction in ionic liquids, *Eur. J. Org. Chem.* 2018 (2018) 1284–1306, <https://doi.org/10.1002/ejoc.201701509>.
- [21] Y.U. Gadhari, N.L. Jadhav, N.T. Hatvate, V.N. Telvekar, Concentrated solar radiation aided green approach for preparative scale and solvent-free synthesis of 3-Methyl-4-(hetero)arylmethylene isoxazole-5(4H)-ones, *ChemistrySelect* 5 (2020) 12320–12323, <https://doi.org/10.1002/slct.202003348>.
- [22] M. Marchi, G. Gentile, C. Rosso, M. Melchionna, P. Fornasiero, G. Filippini, M. Prato, The nickel age in synthetic dual photocatalysis: a bright trip toward materials science, *ChemSusChem* 15 (2022), e202201094.
- [23] Z. She, D. Niu, L. Chen, M.A. Gunawan, X. Shanja, W.H. Hersh, Y. Chen, Synthesis of trisubstituted isoxazoles by palladium(II)-Catalyzed cascade cyclization-alkenylation of 2-Alkyn-1-one O-methyl oximes, *J. Org. Chem.* 77 (2012) 3627–3633, <https://doi.org/10.1021/jo300090k>.
- [24] M. Kurian, D.S. Nair, Heterogeneous Fenton behavior of nano nickel zinc ferrite catalysts in the degradation of 4-chlorophenol from water under neutral conditions, *J. Water Process Eng.* 8 (2015) e37–e49, <https://doi.org/10.1016/j.jwpe.2014.10.011>.
- [25] K.H. Choi, M. Shokouhimehr, Y.E. Sung, Heterogeneous suzuki cross-coupling reaction catalyzed by magnetically recyclable nanocatalyst, *Bull. Kor. Chem. Soc.* 34 (2013) 1477–1480, <https://doi.org/10.5012/bkcs.2013.34.5.1477>.
- [26] M. Nasrollahzadeh, N. Motahharifar, M. Sajjadi, A. Naserimanesh, M. Shokouhimehr, Functionalization of chitosan by grafting Cu(II)-5-amino-1H-tetrazole complex as a magnetically recyclable catalyst for C-N coupling reaction, *Inorg. Chem. Commun.* 136 (2022), 109135, <https://doi.org/10.1016/j.inoche.2021.109135>.
- [27] M. Nasrollahzadeh, N. Shafiei, T. Baran, K. Pakzad, M.R. Tahsili, N.Y. Baran, M. Shokouhimehr, Facile synthesis of Pd nanoparticles supported on a novel Schiff base modified chitosan-kaolin: antibacterial and catalytic activities in Sonogashira coupling reaction, *J. Organomet. Chem.* 945 (2021), 121849, <https://doi.org/10.1016/j.jorganchem.2021.121849>.
- [28] K. Zhang, J. Kim, K.O. Kirlikovali, J. Wang, T.H. Lee, S.Y. Kim, R.S. Varma, H.W. Jang, O.K. Farha, M. Shokouhimehr, Magnetically recyclable nanocomposites via lanthanide-based MOFs grown on natural sea sponge: screening hydrogenation of nitrophenol to aminophenol, *Mol. Catal.* 528 (2022), 112459, <https://doi.org/10.1016/j.mcat.2022.112459>.
- [29] H. Alamgholiloo, N.N. Pesyari, R. Mohammadi, S. Rostamnia, M. Shokouhimehr, Synergistic advanced oxidation process for the fast degradation of ciprofloxacin antibiotics using a GO/CuMOF-magnetic ternary nanocomposite, *J. Environ. Chem. Eng.* 9 (2021), 105486, <https://doi.org/10.1016/j.jece.2021.105486>.
- [30] D. Jagadeesan, *Applied Catalysis A*: general Multifunctional nanocatalysts for tandem reactions: a leap toward sustainability, *Appl. Catal., A* 511 (2016) 59–77, <https://doi.org/10.1016/j.apcata.2015.11.033>.
- [31] R. Bhatt, A.K. Bajpai, Solubility behavior of poly (diaminonaphthalene) doped poly (vinyl alcohol) films in different solvents and structural and electrical characterization of corresponding films, *Mater. Res. Express* 6 (2019), <https://doi.org/10.1088/2053-1591/ab3943>.
- [32] A. Meneguzzi, M.C. Pham, C.A. Ferreira, J.C. Lacroix, S. Aeiych, P.C. Lazace, Electroactive poly(aromatic amine) films deposited on mild steel, *Synth. Met.* 102 (1999) 1390–1391, [https://doi.org/10.1016/S0379-6779\(98\)01020-0](https://doi.org/10.1016/S0379-6779(98)01020-0).
- [33] R. Bhatt, A. Mishra, A.K. Bajpai, Role of diaminonaphthalene based polymers as sensors in detection of biomolecules: a review, *Results Mater* 9 (2021), 100174, <https://doi.org/10.1016/j.rinma.2021.100174>.
- [34] M.S. Tiwari, A.B. Gawade, G.D. Yadav, Magnetically separable sulfated zirconia as highly active acidic catalysts for selective synthesis of ethyl levulinate from furfuryl alcohol, *Green Chem.* 19 (2017) 963–976, <https://doi.org/10.1039/C6GC02466A>.
- [35] S. Shylesh, V. Schünemann, W.R. Thiel, Magnetically separable nanocatalysts: bridges between homogeneous and heterogeneous catalysis, *Angew. Chem. Int. Ed.* 49 (2010) 3428–3459, <https://doi.org/10.1002/anie.200905684>.
- [36] L.M. Rossi, N.J.S. Costa, F.P. Silva, R. Wojcieszak, Magnetic nanomaterials in catalysis: advanced catalysts for magnetic separation and beyond, *Green Chem.* 16 (2014) 2906–2933, <https://doi.org/10.1039/C4GC00164H>.
- [37] S.M. Nezhad, S.A. Pourmousavi, E.N. Zare, G. Heidari, P. Mavvandi, Magnetic sulfonated melamine-Formaldehyde Resin as an efficient catalyst for the synthesis of antioxidant and antimicrobial pyrazolone derivatives, *Catalysts* 12 (2022) 626.
- [38] X.G. Li, M.R. Huang, S.X. Li, Facile synthesis of poly(1,8-diaminonaphthalene) microparticles with a very high silver-ion adsorbability by a chemical oxidative polymerization, *Acta Mater.* 52 (2004) 5363–5374, <https://doi.org/10.1016/j.actamat.2004.07.042>.
- [39] X.G. Li, M.R. Huang, Y.B. Jiang, J. Yu, Z. He, Synthesis of poly(1,5-diaminonaphthalene) microparticles with abundant amino and imino groups as strong adsorbers for heavy metal ions, *Microchim. Acta* 186 (2019), <https://doi.org/10.1007/s00604-019-3330-z>.
- [40] B. Wessling, New insight into organic metal polyaniline morphology and structure, *Polymers* 2 (2010) 786–798.
- [41] M. Higuchi, D. Imoda, T. Hirao, Redox behavior of Polyaniline– transition metal complexes in solution, *Macromolecules* 29 (1996) 8277–8279.
- [42] S.N. Maddila, S. Maddila, W.E. Van Zyl, S.B. Jonnalagadda, Ag/SiO₂ as a recyclable catalyst for the facile green synthesis of 3-methyl-4-(phenyl)methylene-isoxazole-5(4H)-ones, *Res. Chem. Intermed.* 42 (2016) 2553–2566, <https://doi.org/10.1007/s11164-015-2167-2>.
- [43] S.A. Pourmousavi, H.R. Fattahi, F. Ghorbani, A. Kanaani, D. Ajloo, A green and efficient synthesis of isoxazol-5(4H)-one derivatives in water and a DFT study, *J. Iran. Chem. Soc.* 15 (2018) 455–469, <https://doi.org/10.1007/s13738-017-1246-2>.
- [44] Z. Faramarzi, H. Kiyani, Organocatalyzed three-component synthesis of isoxazol-5(4H)-ones under aqueous conditions, *Heterocycles* 102 (2021), <https://doi.org/10.3987/COM-21-14488>.
- [45] M. Ahmadzadeh, Z. Zarnegar, J. Safari, Sonochemical synthesis of methyl-4-(Hetero)arylmethylene isoxazole-5(4H)-ones using Snii-montmorillonite, *Green Chem. Lett. Rev.* 11 (2018) 78–85, <https://doi.org/10.1080/17518253.2018.1434564>.
- [46] Q. Liu, R.T. Wu, Facile synthesis of 3-methyl-4-arylmethylene-isoxazol-5(4H)-ones catalysed by sodium silicate in an aqueous medium, *J. Chem. Res.* 35 (2011) 598–599, <https://doi.org/10.3184/174751911X13176501108975>.
- [47] K. Ablajan, H. Xiamuxi, The convenient synthesis of 4-arylmethylidene-4,5-dihydro-3-phenylisoxazol- 5-ones, *Chin. Chem. Lett.* 22 (2011) 151–154, <https://doi.org/10.1016/j.cclct.2010.09.023>.
- [48] H. Kiyani, H.A. Samimi, Nickel-catalyzed one-pot, three-component synthesis of 3,4-disubstituted isoxazole-5(4H)-ones in aqueous medium, *Chiang Mai J. Sci.* 44 (2017) 1011–1021.
- [49] P. Basak, S. Dey, P. Ghosh, Sulfonated graphene-oxide as metal-free efficient carbocatalyst for the synthesis of 3-Methyl-4-(hetero)arylmethylene isoxazole-5(4H)-ones and substituted pyrazole, *ChemistrySelect* 5 (2020) 626–636, <https://doi.org/10.1002/slct.201904164>.
- [50] S.K. Asadi, G. Aleaba, N. Daneshvar, F. Shirini, Sustainable and green synthesis of 3-methyl-4-arylmethylene-isoxazole-5(4H)-one derivatives under mild conditions using a novel phosphoric acid-based molten salt as catalyst, *Sustain. Chem. Pharm.* 21 (2021), 100442, <https://doi.org/10.1016/j.scp.2021.100442>.
- [51] R. Nongrum, R. Nongkhaw, S.P. Majaw, J. Kumari, D. Sriram, R. Nongkhaw, A nano-organo catalyst mediated approach towards the green synthesis of 3-methyl-4-(phenyl)methylene-isoxazole-5(4H)-one derivatives and biological evaluation of the derivatives as a potent anti-fungal and anti-tubercular agent, *Sustain. Chem. Pharm.* 32 (2023), 100967, <https://doi.org/10.1016/j.scp.2023.100967>.
- [52] Y.R. Girish, K.S. Sharithkumar, K. Prashantha, S. Rangappa, M.S. Sudhanva, Significance of antioxidants and methods to evaluate their potency, *Mater. Chem. Horizons* (2023), <https://doi.org/10.22128/MCH.2023.647.1037>.